

Method for Solving Bang-Bang and Singular Optimal Control Problems using Adaptive Radau Collocation

Elisha R. Pager^{*}

Anil V. Rao[†]

April 27, 2021

Abstract

A method is described for solving bang-bang and singular optimal control problems using adaptive Legendre-Gauss-Radau (LGR) collocation and control regularization. The method consists of three stages including structure detection, structure decomposition, and domain refinement. Structure detection detects discontinuities in the control solution and analyzes the control for bang-bang and singular arcs. After the structure is detected, the problem is decomposed into a multiple-domain formulation and discretized using adaptive LGR collocation. The adaptive LGR collocation allows the time horizon to be partitioned into multiple domains and includes the addition of new decision variables to represent the switch times in the control profile. The last stage introduces additional constraints into the problem corresponding to each domain type. Specifically, a proximal method is enforced when a singular domain is present. The method is demonstrated on four examples, and results indicate that the method solves nonsmooth and/or singular optimal control problems to a higher accuracy when compared with previously developed methods for smooth optimal control.

^{*}Ph.D. Student, Department of Mechanical and Aerospace Engineering, University of Florida, Gainesville, Florida 32611-6250. Email: epager@ufl.edu.

[†]Associate Professor, Department of Mechanical and Aerospace Engineering, University of Florida, Gainesville, FL 32611-6250. E-mail: anilvrao@ufl.edu. Corresponding Author

1 Introduction

Optimal control problems arise frequently in many engineering applications due to the need to optimize the performance of a controlled dynamical system. In general, optimal control problems do not have analytic solutions and must be solved numerically. A key challenge in solving an optimal control problem numerically arises due to the fact that most optimal control problems are subject to constraints on the system. These constraints often take the form of path constraints where limits are imposed on functions of either the control and/or the state. Most constrained optimal control problems have nonsmooth solutions. The nonsmoothness in the solutions arises from instantaneous switches in the control or switches between activity and inactivity in the state path constraints. Beyond the fact that such switches may lie at the limits of either the control or the state, in many problems the solution may lie on one or more singular arcs. The existence of singular arcs makes solving constrained optimal control problems even more challenging because Pontryagin's minimum principle (that is, first and second-order optimality conditions) fail to yield a complete solution along a singular arc. As a result, when applying a computational method to a problem whose solution lies on a singular arc, standard methods produce insensible results. This research is motivated by the importance of solving optimal control problems whose solutions are nonsmooth and singular.

Numerical methods for optimal control fall into two broad categories: indirect methods and direct methods. In an indirect method, the first-order variational optimality conditions are derived, and the optimal control problem is converted to a Hamiltonian boundary-value problem (HBVP). The HBVP is then solved numerically using a differential-algebraic equation solver. In a direct method, the state and control are approximated, and the optimal control problem is transcribed into a finite-dimensional nonlinear programming problem (NLP) [1]. The NLP is then solved numerically using well-developed software such as *SNOPT* or *IPOPT* [2, 3]. While concrete theory has been established for deriving optimal singular control conditions analytically there is still great progress to be made in the area of numerical methods. Much of the current work requires the use of the first-order variational optimality conditions to solve for singular controls. Thus, indirect methods are quite popular for solving singular optimal control problems. However, more recently, direct collocation methods have become increasingly popular in the numerical solution of both smooth and nonsmooth optimal control problems.

Over the past two decades, a particular class of direct methods, called direct collocation methods, has

been used extensively for solving continuous optimal control problems. A direct collocation method is an implicit simulation method where the state and control are parameterized, and the constraints in the continuous optimal control problem are enforced at a specially chosen set of collocation points. In more recent years, a great deal of research has been carried out in the area of *Gaussian quadrature orthogonal collocation methods* [4, 5, 6, 7]. In a Gaussian quadrature method, the state is approximated using a set of Lagrange polynomials where the support points of the polynomials are chosen to be the points associated with a Gaussian quadrature. The most well developed Gaussian quadrature methods employ either Legendre-Gauss (LG) points [4, 8], Legendre-Gauss-Radau (LGR) points [5, 6, 7, 9], or Legendre-Gauss-Lobatto (LGL) points [10]. More recently, a convergence theory has been developed to show that under certain assumptions of smoothness and coercivity, an *hp*-Gaussian quadrature method employing either LG or LGR collocation points will converge to a local minimizer of the optimal control problem at an exponential rate [11, 12, 13, 14, 15]. For these reasons, direct methods should be explored in the effort to develop novel computational methods for singular optimal control.

When a solution is nonsmooth and/or singular, which is often the case for mechanical systems, computational challenges arise. The difficulty is twofold. First, the precise locations of any discontinuities and the structure of the control must be identified. Static mesh refinement methods that employ Gaussian quadrature have been developed as an attempt to address the problem of handling discontinuities in the solution [16, 17, 18]. A more recent idea to solve this problem is the development and use of variable mesh refinement methods and structure detection methods. Unlike classical mesh refinement methods, [19, 20, 21], where the mesh is static, variable mesh refinement methods work by including parameters in the optimization that define the location of the discontinuities. A variable mesh provides a way to obtain an accurate approximation of switch points in the solution. Some examples of previous work on variable mesh refinement methods include [22, 23, 24, 25, 26]. The methods in [22, 23, 24] use the Lagrange multipliers to detect the switch point locations in the control structure and then place variable mesh points to represent the switch points in the NLP, while [25, 26] use the switching function and a sensitivity analysis to place moving finite elements at the switch point locations. In [27], a mesh refinement method for solving bang-bang optimal control problems was developed using the Hamiltonian and the switching function to detect the structure and constrain the bang-bang control accordingly. The work presented in this paper also uses the Hamiltonian

in the structure detection process, but differs from the method in [27] because this work can also detect and approximate singular arcs. In [27], singular arcs are not considered. Additionally, this work uses a different discontinuity detection method to first locate the switch points. More recently, in [28] a switch point algorithm was developed for optimizing over the locations of switch points in a nonsmooth control solution, but a priori knowledge of the switch points existence is required. Furthermore, methods that utilize structure detection on a static mesh are also reported in [29, 30].

The second difficulty stems from determining an accurate approximation to the optimal control on a singular arc. Several approaches have been developed for solving singular optimal control problems using both indirect and direct methods. A majority of these methods typically employ either a regularization approach or use of the optimality conditions with an indirect method to solve for the singular control, see [31, 32, 33]. A regularization method transforms the singular control problem into a series of nonsingular problems by minimizing a penalty term that is a quadratic function of the control and it has been widely developed and implemented in this research area. This approach has been implemented using dynamic programming, indirect methods, direct methods, and nested indirect/direct approaches [31, 34, 35, 36]. More recent implementations of regularization based techniques include the uniform trigonometrization method (UTM) developed in [37] and the use of a continuation method of a regularized term in [38]. The UTM method is an indirect approach that uses trigonometry to determine singular optimal control solutions. Aside from regularization based approaches, research has also been conducted on the use of monotonic control function approximations to reduce the oscillations and numerical challenges observed with singular arcs [25, 26, 39, 40].

Motivated by the prevalence of bang-bang and singular arcs in optimal control solutions and the need for a general method that can handle such solutions, this paper describes a new method for detecting and solving optimal control problems whose solutions are nonsmooth and singular. The method of this paper exploits the advantages of using an adaptive formulation of LGR collocation with a regularization method to accurately detect and solve a singular optimal control problem. Discontinuity detection using jump function approximations [18] combined with Hamiltonian detection is used to analyze the structure of a coarse control solution. The adaptive LGR collocation is used to partition the time horizon into multiple domains with additional decision variables assigned at the detected switch point locations. Each type of domain is then

constrained appropriately and *hp*-adaptive mesh refinement is utilized when necessary. More specifically, in a singular domain the proximal method, first introduced in [41, 42], is applied. The proximal method, also known as a regularization method, that is employed over a singular arc is developed as a variation of the $\epsilon\text{-}\alpha(\cdot)$ algorithm presented in [34], but this paper extends the use of a regularization method to collocation methods. This work differs from that of [34] in two ways. First, in this previous work the singular control is regularized and solved by iterative dynamic programming. Different from this prior research, in this work the proximal method is implemented by a direct method referred to as adaptive LGR collocation. Second, in this current research the proximal method developed is only applied over the time domain containing a singular arc as opposed to the entire time horizon. As a result, this method converges to a highly accurate approximation of the singular control.

The contributions of this work are as follows. The combined use of jump function approximations and the numerically computed switching function are applied to detect the presence of discontinuities, bang-bang arcs, and singular arcs. Furthermore, no information regarding the nonsmooth or singular structure is required. The next contribution is extending the use of regularization methods to direct collocation methods. The adaptive LGR collocation and structure detection allows the method to only regularize over singular intervals, making the control regularization more precise and effective. In applying the method developed in this work, enforcing Pontryagin's minimum principal to derive the singular feedback control law is avoided. This is important because generally the derived singular control is a function of the states and the costates. If this is the case then it cannot be implemented using a direct method as the NLP resulting from direct collocation only produces estimates of the NLP multipliers. Moreover, the proximal method is also able to solve problems whose solutions are singular arcs of infinite order. Computational benefits gained by employing the new method are demonstrated on four examples as the final contribution.

The remainder of the paper is organized as follows. Section 2 introduces the Bolza optimal control problem and the necessary conditions for optimality. Section 3 describes the adaptive Legendre-Gauss-Radau collocation method used to transcribe the multiple-domain Bolza optimal control problem. A brief overview of nonsmooth optimal control is provided in Section 4. The method for solving bang-bang and singular optimal control problems is detailed in Section 5 and 6. The method is then demonstrated on four examples in Section 7. Finally, Section 8 gives concluding remarks.

2 Optimal Control Problem

Without loss of generality, consider the following single-phase optimal control problem in Bolza form defined on the time horizon $t \in [t_0, t_f]$. Determine the state $\mathbf{x}(t) \in \mathbb{R}^1 \times n_x$, the control $\mathbf{u}(t) \in \mathbb{R}^1 \times n_u$, and the terminal time $t_f \in \mathbb{R}$ that minimize the objective functional

$$\mathcal{J} = \mathcal{M}(\mathbf{x}(t_0), t_0, \mathbf{x}(t_f), t_f) + \int_{t_0}^{t_f} \mathcal{L}(\mathbf{x}(t), \mathbf{u}(t), t) dt, \quad (1)$$

subject to the dynamic constraints

$$\frac{d\mathbf{x}(t)}{dt} \equiv \dot{\mathbf{x}}(t) = \mathbf{a}(\mathbf{x}(t), \mathbf{u}(t), t), \quad (2)$$

the path constraints

$$\mathbf{c}_{\min} \leq \mathbf{c}(\mathbf{x}(t), \mathbf{u}(t), t) \leq \mathbf{c}_{\max}, \quad (3)$$

and the boundary conditions

$$\mathbf{b}_{\min} \leq \mathbf{b}(\mathbf{x}(t_0), t_0, \mathbf{x}(t_f), t_f) \leq \mathbf{b}_{\max}, \quad (4)$$

where the functions \mathcal{M} , \mathcal{L} , \mathbf{a} , \mathbf{b} , and \mathbf{c} are defined by the mappings

$$\mathcal{M} : \mathbb{R}^{n_x} \times \mathbb{R} \times \mathbb{R}^{n_x} \times \mathbb{R} \rightarrow \mathbb{R},$$

$$\mathcal{L} : \mathbb{R}^{n_x} \times \mathbb{R}^{n_u} \times \mathbb{R} \rightarrow \mathbb{R},$$

$$\mathbf{a} : \mathbb{R}^{n_x} \times \mathbb{R}^{n_u} \times \mathbb{R} \rightarrow \mathbb{R}^{n_x},$$

$$\mathbf{c} : \mathbb{R}^{n_x} \times \mathbb{R}^{n_u} \times \mathbb{R} \rightarrow \mathbb{R}^{n_c}.$$

$$\mathbf{b} : \mathbb{R}^{n_x} \times \mathbb{R} \times \mathbb{R}^{n_x} \times \mathbb{R} \rightarrow \mathbb{R}^{n_b}.$$

The Bolza optimal control problem given in Eqs. (1)–(4) gives rise to the following first-order calculus of variations [43, 44, 45] conditions:

$$\dot{\mathbf{x}}(t) = \frac{\partial \mathcal{H}}{\partial \boldsymbol{\lambda}(t)}, \quad (5)$$

$$\dot{\boldsymbol{\lambda}}(t) = -\frac{\partial \mathcal{H}}{\partial \mathbf{x}(t)}, \quad (6)$$

$$\mathbf{u}^*(t) = \arg \min_{\mathbf{u} \in \mathcal{U}} \mathcal{H}(\mathbf{x}, \boldsymbol{\lambda}, \boldsymbol{\mu}, \mathbf{u}, t), \quad (7)$$

where $\boldsymbol{\lambda}(t) \in \mathbb{R}^{n_x}$ is the costate, $\boldsymbol{\mu}(t) \in \mathbb{R}^{n_c}$ is the path constraint multiplier

$$\mathcal{H}(\mathbf{x}, \boldsymbol{\lambda}, \boldsymbol{\mu}, \mathbf{u}, t) = \mathcal{L}(\mathbf{x}(t), \mathbf{u}(t), t) + \boldsymbol{\lambda}^\top(t) \mathbf{a}(\mathbf{x}(t), \mathbf{u}(t), t) - \boldsymbol{\mu}^\top(t) \mathbf{c}(\mathbf{x}(t), \mathbf{u}(t), t), \quad (8)$$

is the control Hamiltonian, and \mathcal{U} is the admissible control set. The transversality conditions are given by

$$\boldsymbol{\lambda}(t_0) = -\frac{\partial \mathcal{M}}{\partial \mathbf{x}(t_0)} + \boldsymbol{\nu}^\top \frac{\partial \mathbf{b}}{\partial \mathbf{x}(t_0)} \quad , \quad \boldsymbol{\lambda}(t_f) = \frac{\partial \mathcal{M}}{\partial \mathbf{x}(t_f)} - \boldsymbol{\nu}^\top \frac{\partial \mathbf{b}}{\partial \mathbf{x}(t_f)} \quad (9)$$

$$\mathcal{H}(t_0) = \frac{\partial \mathcal{M}}{\partial t_0} - \boldsymbol{\nu}^\top \frac{\partial \mathbf{b}}{\partial t_0} \quad , \quad \mathcal{H}(t_f) = -\frac{\partial \mathcal{M}}{\partial t_f} + \boldsymbol{\nu}^\top \frac{\partial \mathbf{b}}{\partial t_f} \quad (10)$$

$$\mu_j(t) = 0, \text{ when } c_j(\mathbf{x}, \mathbf{u}, t) < 0, \quad j = 1, \dots, p \quad (11)$$

$$\mu_j(t) \leq 0, \text{ when } c_j(\mathbf{x}, \mathbf{u}, t) = 0, \quad j = 1, \dots, p$$

where $\boldsymbol{\nu}$ is the Lagrange multiplier associated with the boundary conditions. Equations (5) and (6) form what is classically known as a *Hamiltonian system* [43, 44]. Equation (7) is known as *Pontryagin's Minimum Principle* [46] (PMP) and is used to determine the optimal control as a function of the state and costate. The conditions in Eqs. (9) and (10) are called *transversality conditions* [43, 44, 45] on the boundary values of the costate, while the conditions given in Eq. (11) are the *complementary slackness conditions* [47, 48] on the path constraints. The Hamiltonian system, together with the original boundary conditions, the costate transversality conditions, and complementary slackness conditions, forms a *Hamiltonian boundary-value problem* (HBVP) [43, 44, 45]. Any solution $(\mathbf{x}(t), \boldsymbol{\lambda}(t), \mathbf{u}(t), \boldsymbol{\mu}(t), \boldsymbol{\nu})$ to the HBVP is called an *extremal* solution. A solution to the HBVP is typically found using an indirect method.

3 Adaptive Legendre-Gauss-Radau Collocation

Direct collocation is used to discretize the continuous optimal control problem. In particular, the previously developed *hp*-adaptive Legendre-Gauss-Radau (LGR) collocation method [5, 6, 7, 9, 15, 21] is used because it has been shown to produce accurate approximations of the state, control, and costate while converging exponentially for smooth solutions. However, the focus of this paper is solving for nonsmooth solutions thus modifications to the standard LGR formulation are made.

For this research a multiple-domain formulation of the LGR collocation method with added decision variables is derived and referred to as adaptive LGR collocation. This formulation divides the problem into domains based on the results of a structure detection algorithm. The continuous-time Bolza optimal control problem described in Eqs. (1)–(4) is discretized using collocation at the Legendre-Gauss-Radau (LGR) points [5, 6, 7, 9]. The time horizon $t \in [t_0, t_f]$ may be divided into D time domains, $\mathcal{P}_d = [t_s^{[d-1]}, t_s^{[d]}] \subseteq$

$[t_0, t_f]$, $d \in \{1, \dots, D\}$, such that

$$\bigcup_{d=1}^D \mathcal{P}_d = [t_0, t_f] , \quad \bigcap_{d=1}^D \mathcal{P}_d = \{t_s^{[1]}, \dots, t_s^{[D-1]}\} , \quad (12)$$

where $t_s^{[d]}$, $d \in \{1, \dots, D-1\}$ are the domain interface variables of the problem, $t_s^{[0]} = t_0$, and $t_s^{[D]} = t_f$. Thus, in the case where $D = 1$ the phase consists of only a single domain $\mathcal{P}_1 = [t_0, t_f]$ and $\{t_s^{[1]}, \dots, t_s^{[D-1]}\} = \emptyset$. The domain interface variables are also defined as, $t_s^{[d]}$, $s \in \{1, \dots, S\}$, where the set of time variables represent the switch point times in the control structure and S is the total number of domain interface variables. In the adaptive LGR collocation method, each of the time domains $\mathcal{P}_d = [t_s^{[d-1]}, t_s^{[d]}]$, $d \in \{1, \dots, D\}$, are mapped to the set $\tau \in [-1, +1]$ using the affine transformation,

$$\begin{aligned} t &= \frac{t_s^{[d]} - t_s^{[d-1]}}{2} \tau + \frac{t_s^{[d]} + t_s^{[d-1]}}{2} , \\ \tau &= 2 \frac{t - t_s^{[d-1]}}{t_s^{[d]} - t_s^{[d-1]}} - 1 . \end{aligned} \quad (13)$$

The interval $\tau \in [-1, +1]$ for each domain \mathcal{P}_d is then divided into K mesh intervals, $\mathcal{S}_k = [T_{k-1}, T_k] \subseteq [-1, +1]$, $k \in \{1, \dots, K\}$ such that

$$\bigcup_{k=1}^K \mathcal{S}_k = [-1, +1] , \quad \bigcap_{k=1}^K \mathcal{S}_k = \{T_1, \dots, T_{K-1}\} , \quad (14)$$

and $-1 = T_0 < T_1 < \dots < T_{K-1} < T_K = +1$. For each mesh interval, the LGR points used for collocation are defined in the domain of $[T_{k-1}, T_k]$ for $k \in \{1, \dots, K\}$. The state of the continuous optimal control problem is then approximated in mesh interval \mathcal{S}_k , $k \in \{1, \dots, K\}$, as

$$\mathbf{x}^{(k)}(\tau) \approx \mathbf{X}^{(k)}(\tau) = \sum_{j=1}^{N_k+1} \mathbf{X}_j^{(k)} \ell_j^{(k)}(\tau) , \quad \ell_j^{(k)}(\tau) = \prod_{\substack{l=1 \\ l \neq j}}^{N_k+1} \frac{\tau - \tau_l^{(k)}}{\tau_j^{(k)} - \tau_l^{(k)}} , \quad (15)$$

where $\ell_j^{(k)}(\tau)$ for $j \in \{1, \dots, N_k + 1\}$ is a basis of Lagrange polynomials on \mathcal{S}_k , $(\tau_1^{(k)}, \dots, \tau_{N_k}^{(k)})$ are the set of N_k Legendre-Gauss-Radau (LGR) collocation points in the interval $[T_{k-1}, T_k]$, $\tau_{N_k+1}^{(k)} = T_k$ is a non-collocated support point, and $\mathbf{X}_j^{(k)} \equiv \mathbf{X}^{(k)}(\tau_j^{(k)})$. Differentiating $\mathbf{X}^{(k)}(\tau)$ in Eq. (15) with respect to τ gives

$$\frac{d\mathbf{X}^{(k)}(\tau)}{d\tau} = \sum_{j=1}^{N_k+1} \mathbf{X}_j^{(k)} \frac{d\ell_j^{(k)}(\tau)}{d\tau} . \quad (16)$$

The dynamics are then approximated at the N_k LGR points in mesh interval $k \in \{1, \dots, K\}$ as

$$\sum_{j=1}^{N_k+1} D_{lj}^{(k)} \mathbf{X}_j^{(k)} - \frac{t_f - t_0}{2} \mathbf{a}(\mathbf{X}_l^{(k)}, \mathbf{U}_l^{(k)}, t(\tau_l^{(k)}, t_0, t_f)) = \mathbf{0} , \quad l \in \{1, \dots, N_k\} , \quad (17)$$

where

$$D_{lj}^{(k)} = \frac{d\ell_j^{(k)}(\tau_l^{(k)})}{d\tau}, \quad l \in \{1, \dots, N_k\}, \quad j \in \{1, \dots, N_k + 1\},$$

are the elements of the $N_k \times (N_k + 1)$ *Legendre-Gauss-Radau differentiation matrix* in mesh interval \mathcal{S}_k , $k \in \{1, \dots, K\}$, and $\mathbf{U}_l^{(k)}$ is the approximation of the control at the l^{th} collocation point in mesh interval \mathcal{S}_k . The time variables t_0 and t_f in Eq. (17) represent the initial and final domain interface variables, $t_s^{[d-1]}$ and $t_s^{[d]}$, on the domain \mathcal{P}_d . It is noted that continuity in the state and time between mesh intervals \mathcal{S}_{k-1} and \mathcal{S}_k , $k \in \{1, \dots, K\}$, is enforced by using the same variables to represent $\mathbf{X}_{N_{k-1}+1}^{(k-1)}$ and $\mathbf{X}_1^{(k)}$, while continuity in the state between the domains \mathcal{P}_{d-1} and \mathcal{P}_d , $d \in \{2, \dots, D\}$, is achieved by using the same variables to represent $\mathbf{X}_{N^{[d-1]}+1}^{[d-1]}$ and $\mathbf{X}_1^{[d]}$ where the superscript $[d]$ is used to denote the d^{th} time domain, $\mathbf{X}_j^{[d]}$ denotes the value of the state approximation at the j^{th} discretization point in the time domain \mathcal{P}_d , and $N^{[d]}$ is the total number of collocation points used in time domain \mathcal{P}_d computed by

$$N^{[d]} = \sum_{k=1}^{K^{[d]}} N_k^{[d]}. \quad (18)$$

The Legendre-Gauss-Radau approximation of the multiple-domain optimal control problem results in the following nonlinear programming problem (NLP). Minimize the objective function

$$\mathcal{J} = \mathcal{M}(\mathbf{X}_1^{[1]}, t_0, \mathbf{X}_{N^{[D]}+1}^{[D]}, t_f) + \sum_{d=1}^D \frac{t_s^{[d]} - t_s^{[d-1]}}{2} [\mathbf{w}^{[d]}]^\top \mathbf{L}^{[d]}, \quad (19)$$

subject to the collocated dynamic constraints

$$\Delta^{[d]} = \mathbf{D}^{[d]} \mathbf{X}^{[d]} - \frac{t_s^{[d]} - t_s^{[d-1]}}{2} \mathbf{A}^{[d]} = \mathbf{0}, \quad d \in \{1, \dots, D\}, \quad (20)$$

the path constraints

$$\mathbf{c}_{\min} \leq \mathbf{C}_j^{[d]} \leq \mathbf{c}_{\max}, \quad j \in \{1, \dots, N^{[d]}\}, \quad d \in \{1, \dots, D\}, \quad (21)$$

the boundary conditions

$$\mathbf{b}_{\min} \leq \mathbf{b}(\mathbf{X}_1^{[1]}, t_0, \mathbf{X}_{N^{[D]}+1}^{[D]}, t_f) \leq \mathbf{b}_{\max}. \quad (22)$$

and the continuity constraints

$$\mathbf{X}_{N^{[d-1]}+1}^{[d-1]} = \mathbf{X}_1^{[d]}, \quad d \in \{2, \dots, D\}, \quad (23)$$

noting that Eq. (23) is implicitly satisfied by employing the same variable in the NLP for $\mathbf{X}_{N^{[d-1]}+1}^{[d-1]}$ and $\mathbf{X}_1^{[d]}$. The matrices in Eqs. (19)–(21) are defined as follows

$$\mathbf{A}^{[d]} = \begin{bmatrix} \mathbf{a}(\mathbf{X}_1^{[d]}, \mathbf{U}_1^{[d]}, t_1^{[d]}) \\ \vdots \\ \mathbf{a}(\mathbf{X}_{N^{[d]}}^{[d]}, \mathbf{U}_{N^{[d]}}^{[d]}, t_{N^{[d]}}^{[d]}) \end{bmatrix} \in \mathbb{R}^{N^{[d]} \times n_x}, \quad (24)$$

$$\mathbf{C}^{[d]} = \begin{bmatrix} \mathbf{c}(\mathbf{X}_1^{[d]}, \mathbf{U}_1^{[d]}, t_1^{[d]}) \\ \vdots \\ \mathbf{c}(\mathbf{X}_{N^{[d]}}^{[d]}, \mathbf{U}_{N^{[d]}}^{[d]}, t_{N^{[d]}}^{[d]}) \end{bmatrix} \in \mathbb{R}^{N^{[d]} \times n_c}, \quad (25)$$

$$\mathbf{L}^{[d]} = \begin{bmatrix} \mathcal{L}(\mathbf{X}_1^{[d]}, \mathbf{U}_1^{[d]}, t_1^{[d]}) \\ \vdots \\ \mathcal{L}(\mathbf{X}_{N^{[d]}}^{[d]}, \mathbf{U}_{N^{[d]}}^{[d]}, t_{N^{[d]}}^{[d]}) \end{bmatrix} \in \mathbb{R}^{N^{[d]} \times 1}, \quad (26)$$

$\mathbf{D}^{[d]} \in \mathbb{R}^{N^{[d]} \times [N^{[d]}+1]}$ is the LGR differentiation matrix in time domain \mathcal{P}_d , $d \in \{1, \dots, D\}$, and $\mathbf{w}^{[d]} \in \mathbb{R}^{N^{[d]} \times 1}$ are the LGR weights at each node in time domain \mathcal{P}_d , $d \in \{1, \dots, D\}$. It is noted that $\mathbf{a} \in \mathbb{R}^1 \times n_x$, $\mathbf{c} \in \mathbb{R}^1 \times n_c$, and $\mathcal{L} \in \mathbb{R}^1 \times 1$ correspond, respectively, to the vector fields that define the right-hand side of the dynamics, the path constraints, and the integrand of the optimal control problem, where n_c is the number of path constraints in the problem. Additionally, the state matrix, $\mathbf{X}^{[d]} \in \mathbb{R}^{[N^{[d]}+1] \times n_x}$, and the control matrix, $\mathbf{U}^{[d]} \in \mathbb{R}^{N^{[d]} \times n_u}$, in time domain \mathcal{P}_d , $d \in \{1, \dots, D\}$, are formed as

$$\mathbf{X}^{[d]} = \begin{bmatrix} \mathbf{X}_1^{[d]} \\ \vdots \\ \mathbf{X}_{N^{[d]}+1}^{[d]} \end{bmatrix} \text{ and } \mathbf{U}^{[d]} = \begin{bmatrix} \mathbf{U}_1^{[d]} \\ \vdots \\ \mathbf{U}_{N^{[d]}}^{[d]} \end{bmatrix}, \quad (27)$$

respectively, where n_u is the number of control components and n_x is the number of state components in the problem.

3.1 Costate Estimation

Estimates of the costate may be obtained at each of the discretization points in the time domain $\mathcal{P}_d, d \in \{1, \dots, D\}$, using the transformation, see [49],

$$\begin{aligned} \boldsymbol{\lambda}^{[d]} &= (\mathbf{W}^{[d]})^{-1} \boldsymbol{\Lambda}^{[d]}, \\ \boldsymbol{\lambda}_{N^{[d]}+1}^{[d]} &= (\mathbf{D}_{N^{[d]}+1}^{[d]})^\top \boldsymbol{\Lambda}^{[d]}, \end{aligned} \quad (28)$$

where $\boldsymbol{\lambda}^{[d]} \in \mathbb{R}^{N^{[d]} \times n_x}$ is a matrix of the costate estimates at the collocation points in time domain \mathcal{P}_d , $\mathbf{W}^{[d]} = \text{diag}(\mathbf{w}^{[d]})$ is a diagonal matrix of the LGR weights at the collocation points in time domain \mathcal{P}_d , $\mathbf{\Lambda}^{[d]} \in \mathbb{R}^{N^{[d]} \times n_x}$ is a matrix of the NLP multipliers obtained from the NLP solver corresponding to the defect constraints at the collocation points in time domain \mathcal{P}_d , $\boldsymbol{\lambda}_{N^{[d]}+1}^{[d]} \in \mathbb{R}^{1 \times n_x}$ is a row vector of the costate estimates at the non-located end point in time domain \mathcal{P}_d , and $\mathbf{D}_{N^{[d]}+1}^{[d]} \in \mathbb{R}^{N^{[d]} \times 1}$ is the last column of the LGR differentiation matrix in time domain \mathcal{P}_d .

3.2 Summary

In summary, a single *phase* problem on $t \in [t_0, t_f]$ is divided into D domains, $\mathcal{P}_d = [t_s^{[d-1]}, t_s^{[d]}]$, $d \in \{1, \dots, D\}$, that are then mapped to the interval $\tau^{[d]} \in [-1, +1]$. The interval $\tau^{[d]} \in [-1, +1]$ for each domain is then divided into K mesh intervals, $\mathcal{S}_k = [T_{k-1}, T_k] \subseteq [-1, +1]$, $k \in \{1, \dots, K\}$. The intersection of each domain is determined by the *domain interface variables*, $t_s^{[d]}$, $s \in \{1, \dots, S\}$.

4 Nonsmooth and Singular Optimal Control

The term nonsmooth is used to denote the optimal control as displaying both nonsmooth and singular behavior. By definition a singular arc will occur in a solution when the application of Pontryagin's minimum principle fails to yield a complete solution of the optimal control [45]. This phenomena can occur in many situations but is most common when the dynamics are linear in the control and the control is bounded, or the Hamiltonian is not an explicit function of time. It should be noted that singular arcs can also occur in other situations, but in order to provide structure to the method developed in this paper, only problems that fall into the aforementioned categories will be considered.

For simplicity, it is assumed that the control is scalar, $u(t) \in \mathbb{R}$. Suppose the optimal control problem described in Eqs. (1)–(4) is nonsmooth and singular as defined by the assumptions mentioned previously. The following constraint on the control will also be considered

$$u_{\min} \leq u(t) \leq u_{\max}. \quad (29)$$

The dynamics can now be rewritten in the affine form as

$$\dot{\mathbf{x}}(t) = \mathbf{a}(\mathbf{x}(t), u(t)) = \mathbf{g}(\mathbf{x}(t)) + \mathbf{h}(\mathbf{x}(t))u(t), \quad (30)$$

where $\mathbf{g}(\mathbf{x}(t))$ and $\mathbf{h}(\mathbf{x}(t))$ are not functions of the control. The Hamiltonian from Eq. (8) is redefined as

$$\mathcal{H}(\mathbf{x}, \boldsymbol{\lambda}, \boldsymbol{\mu}, u) = \mathbf{f}(\mathbf{x}(t), \boldsymbol{\lambda}(t)) + \boldsymbol{\phi}^\top(\mathbf{x}(t), \boldsymbol{\lambda}(t))u(t) + \boldsymbol{\mu}^\top(t)\mathbf{c}(\mathbf{x}(t), t), \quad (31)$$

where $\mathbf{f}(\mathbf{x}(t), \boldsymbol{\lambda}(t))$ and $\boldsymbol{\phi}(\mathbf{x}(t), \boldsymbol{\lambda}(t))$ are the components of the Hamiltonian that are not a function of the control, and mixed state and control path constraints are not considered. The strong form of Pontryagin's Minimum Principle (PMP), Eq. (7), is applied as follows

$$\frac{\partial \mathcal{H}}{\partial u} = \mathcal{H}_u = \boldsymbol{\phi}(\mathbf{x}(t), \boldsymbol{\lambda}(t)) = 0. \quad (32)$$

Note that the control does not appear in Eq. (32) because the Hamiltonian is linear in the control. A singular arc is characterized as $\mathcal{H}_u = 0$ and \mathcal{H}_{uu} is singular everywhere on the arc. When this occurs, the reduced Hessian matrix associated with the corresponding NLP that arises from the direct transcription method of Section 3 is ill-conditioned such that the projected Hessian matrix is not positive definite. This leads to poor conditioning in the control profiles which often presents itself in the form of oscillations, or chattering behavior, in the control solution.

The sign and value of $\boldsymbol{\phi}(\mathbf{x}(t), \boldsymbol{\lambda}(t))$, also known as the switching function, determines if the control is called a *bang-bang* control or a *singular* control. The weak form of PMP [45] is used in the case of nonsmooth control and the minimization of the Hamiltonian leads to the following piecewise-continuous control, $u(t)$, that is dependent on the switching function as follows

$$u^* = \arg \min_{u(t) \in \mathcal{U}} \mathcal{H} = \begin{cases} u_{\min} & , \quad \boldsymbol{\phi}(\mathbf{x}(t), \boldsymbol{\lambda}(t)) > 0, \\ u_{\text{singular}} & , \quad \boldsymbol{\phi}(\mathbf{x}(t), \boldsymbol{\lambda}(t)) = 0, \\ u_{\max} & , \quad \boldsymbol{\phi}(\mathbf{x}(t), \boldsymbol{\lambda}(t)) < 0, \end{cases} \quad (33)$$

where the sign of the switching function, $\boldsymbol{\phi}(\mathbf{x}(t), \boldsymbol{\lambda}(t))$, is determined by the state and the costate, and $\mathcal{U} \in [u_{\min}, u_{\max}]$ is the admissible control set. As the switching function $\boldsymbol{\phi}(\mathbf{x}(t), \boldsymbol{\lambda}(t))$ changes sign, the control coincides with the sign changes by switching between its maximum and minimum values. Any time interval over which $\boldsymbol{\phi}(\mathbf{x}(t), \boldsymbol{\lambda}(t))$ is zero is referred to as a singular arc and any control in the admissible control set will minimize the Hamiltonian. Furthermore, switching between nonsingular and singular arcs give rise to discontinuities on the state and control profiles, and the location of these transition points are referred to as *switch points*. The numerical challenges created by these discontinuities and non-uniqueness issues are illustrated in Fig. 1.

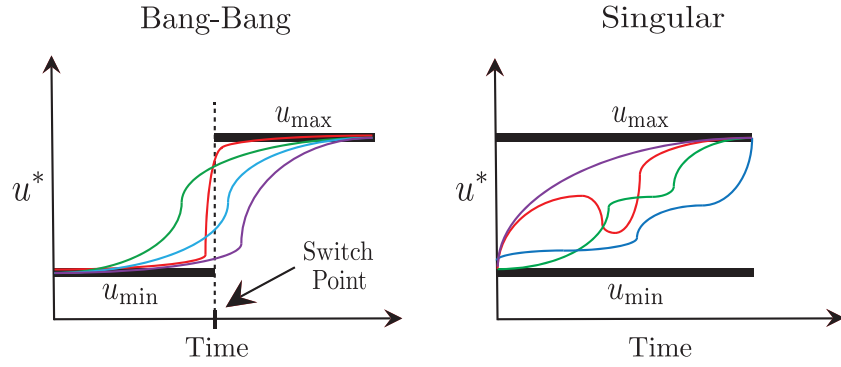


Figure 1: Numerical difficulties associated with bang-bang and singular control solutions.

A common approach to determine unique singular controls over an arc is to repeatedly differentiate \mathcal{H}_u with respect to time until the control explicitly appears. An additional necessary condition for optimality is introduced to guarantee that the resulting singular control law is optimal. This condition is also referred to as the generalized Legendre-Clebsch condition [45, 50, 51, 52],

$$(-1)^k \frac{\partial}{\partial u} \left[\frac{d^{2k}}{dt^{2k}} \mathcal{H}_u \right] \geq 0, \quad (k = 0, 1, 2, \dots), \quad (34)$$

where k represents the order of the singular arc. While in some problems of interest it is possible to use Eq. (34) to determine a condition for the singular control, in many cases Eq. (34) is unable to produce the singular control (for example, if the order of the singular arc is infinite). Even in cases where the singular control could be determined from Eq. (34), taking derivatives higher than second-order is not easy to implement numerically or algorithmically. As mentioned previously, the singular control might be a function of both the state and the costate. If this is the case then a direct collocation method could not be utilized to determine the optimal trajectory. The research presented here is oriented towards developing a fully-automated algorithm that can detect and approximate bang-bang and singular controls. Therefore, having to analytically determine the singular arc condition is not feasible.

5 Method for Solving Bang-Bang and Singular Optimal Control Problems

In this section the method for solving bang-bang and singular optimal control problems is developed. The method consists of several stages. The first stage of the method described in Section 5.1 details the detection of discontinuity points in the control structure and the implementation of Hamiltonian detection if discontinuities are found. The second stage described in Section 5.2 details the decomposition of the optimal control problem into a multiple-domain optimal control problem dictated by the discontinuities detected that are represented as domain interface variables. These domain interface variables are then treated as additional decision variables in the nonlinear programming problem (NLP). In the final stage, new constraints are added to the NLP depending on the Hamiltonian detection's classification of a domain as being bang-bang or singular in order to constrain the modified optimal control problem correctly. The constraints and methods applied in each type of domain are provided in Sections 5.3.1, 5.3.2, and 5.3.3.

5.1 Structure Detection

Assume now that the optimal control problem formulated in Section 2 under the assumptions of Section 4 has been transcribed into a NLP using adaptive LGR collocation developed in Section 3. Note that $D = 1$ meaning a single domain is used for the initial problem. Furthermore, assume that the resulting NLP has been solved to obtain estimates of the state, control, and costate as given in Eqs. (27) and (28), and that the mesh refinement accuracy tolerance has not been satisfied, and thus mesh refinement is required. As a result, it is possible that the solution structure may contain bang-bang and singular arcs, and structure detection is required.

Structure detection detects and locates discontinuities identified on the initial mesh and then uses the locations of the discontinuities to determine the classification of the interval formed by two adjacent discontinuities. In this work, only control discontinuities are considered since only problems where the Hamiltonian is linear in control are analyzed. Their locations are estimated using jump function approximations [18] and then the structure formed by each discontinuity is analyzed using Hamiltonian detection. Structure detection begins by applying the method of Section 5.1.1 to identify and estimate the locations of any control

discontinuities. After discontinuity locations have been estimated, the method of Section 5.1.2 takes the estimated discontinuity locations and determines the classification of the domain as bang-bang or singular. Detailed descriptions of the structure detection process are described next.

5.1.1 Discontinuity Detection

Discontinuities in each control component are detected using jump function approximations of the control solution as shown in [18] because they are an effective tool for estimating areas of nonsmooth behavior in an optimal control solution. A brief summary of the process is now described, but more details can be found in [18]. The jump function approximations are constructed from the numerical control solution and are of the form described in [18].

According to Ref. [53] the jump function of a function $f(t)$ is approximated by

$$L_m f(t) = \frac{1}{q_m(t)} \sum_{t_j \in \mathcal{S}_t} c_j(t) f(t_j) \approx [f](t), \quad (35)$$

where $q_m(t)$ is defined by

$$q_m(t) = \sum_{t_j \in \mathcal{S}_t^+} c_j(t), \quad (36)$$

$c_j(t)$ is defined by

$$c_j(t) = \frac{m!}{\prod_{\substack{i=1 \\ i \neq j}}^{m+1} (t_j - t_i)}, \quad (37)$$

and m specifies the order of the approximation. Higher order approximations converge to the jump function faster outside the neighborhood of discontinuities but have oscillatory behavior in the vicinity of discontinuities. The oscillations are reduced via the **minmod** function, defined here as

$$MM(L_{\mathcal{M}} f(t)) = \begin{cases} \min_{m \in \mathcal{M}} L_m f(t) & \text{if } L_m f(t) > 0 \quad \forall m \in \mathcal{M}, \\ \max_{m \in \mathcal{M}} L_m f(t) & \text{if } L_m f(t) < 0 \quad \forall m \in \mathcal{M}, \\ 0 & \text{otherwise,} \end{cases} \quad (38)$$

where $\mathcal{M} \subset \mathbb{N}^+$ is a finite set of choices of the approximation order m .

Suppose an initial control solution is obtained. The control solution, $U(\tau_j^{(k)}), j = 1, \dots, N_k, k = 1, \dots, K$, is normalized to the interval $[0, 1)$ by the transformation

$$u(\tau_j^{(k)}) = \frac{U(\tau_j^{(k)}) - U_{\min}}{1 + U_{\max} - U_{\min}}, \quad (39)$$

where U_{\min} and U_{\max} are the minimum and maximum values of the control. Together, the normalized control solution and the corresponding collocation points, $\tau_j^{(k)}$ on $[-1, 1)$ of the initial mesh, are applied to Eqs. (35)–(38) to produce a jump function approximation for the normalized control. The jump function approximation is then evaluated at the points $\tau_{j+\frac{1}{2}}^{(k)} = \frac{1}{2}(\tau_j^{(k)} + \tau_{j+1}^{(k)})$, $j = 1, \dots, N_k$, $k = 1, \dots, K$. Let the evaluation of the jump function approximation at $\tau_{j+\frac{1}{2}}^{(k)}$ be denoted by $MM(\tau_{j+\frac{1}{2}}^{(k)})$. The method detects a discontinuity at the location, $\tau_{j+\frac{1}{2}}^{(k)}$, if the condition

$$\left| MM(\tau_{j+\frac{1}{2}}^{(k)}) \right| \geq \eta, \quad (40)$$

is satisfied where the user-defined threshold, $\eta \in (0, 1)$, specifies the relative size of jumps that are detected. The smaller the value of η is the more likely discontinuities present in the solution will be identified; however, the risk of false positives also increases. The opposite can be said for larger values of η .

The discontinuity method of [18] also provides bounds on the uncertainties in the discontinuity locations that are estimated. These bounds are useful because later on they will also be used to determine bounds on the domain interface variables. Consider for some $j = \{1, \dots, N_k\}$ and $k = \{1, \dots, K\}$ that Eq. (40) is satisfied, indicating that a discontinuity is present somewhere on the mesh interval $\tau \in [\tau_j^{(k)}, \tau_{j+1}^{(k)}]$. To account for the uncertainty incurred by using the numerical solution as a sample for the jump function approximation, a safety factor, $\mu \geq 1$ is introduced to extend the uncertainty bounds estimated for the discontinuity. This safety factor provides a larger threshold to adequately capture the potential search space of the estimated switch points. These bound estimates are defined as

$$\begin{aligned} d^- &= \tau_{j+\frac{1}{2}}^{(k)} - \mu \left(\tau_{j+\frac{1}{2}}^{(k)} - \tau_j^{(k)} \right), \\ d^+ &= \tau_{j+\frac{1}{2}}^{(k)} + \mu \left(\tau_{j+1}^{(k)} - \tau_{j+\frac{1}{2}}^{(k)} \right). \end{aligned} \quad (41)$$

Larger values of μ are more desirable as it is more likely that the bounds produced will capture the optimal value of the switch point on the next solution iteration.

5.1.2 Hamiltonian Detection

Hamiltonian detection is employed to determine the structure of the control using the discontinuities identified from the jump function approximations. Specifically, the control solution is inspected to determine if any bang-bang or singular arcs exist. Hamiltonian detection takes the first and second derivatives of the Hamiltonian with respect to control and detects if the Hamiltonian is linear in the control by assessing if the

second derivatives are zero. If the Hamiltonian is affine in control, the first derivatives are computed and represent the switching function of the system. If the Hamiltonian is not linear in the control the structure detection process is finished and smooth mesh refinement, see Section 5.3.3, can take place.

Suppose the initial solution contains the following newly identified discontinuities d_i , $i = 1, \dots, n_d$ and corresponding uncertainty bounds $\{d_i^-, d_i^+\}$, $i = 1, \dots, n_d$. The solution is split into intervals starting with the initial time, the discontinuity locations, and ending with the final time, $\{[-1, d_1], [d_1, d_i], \dots, [d_i, d_{i+1}], [d_{i+1}, +1]\}$, $i = 1, \dots, n_d$. Next, the Hamiltonian in Eq. (31) is computed using the initial solution

$$\mathcal{H}(\mathbf{X}, \boldsymbol{\lambda}, \boldsymbol{\mu}, U) = \mathbf{f}(\mathbf{X}(\tau), \boldsymbol{\lambda}(\tau)) + \boldsymbol{\phi}^\top(\mathbf{X}(\tau), \boldsymbol{\lambda}(\tau))U(\tau) + \boldsymbol{\mu}^\top(\tau)\mathbf{c}(\mathbf{X}(\tau), \tau). \quad (42)$$

Note that the costates are also obtained when solving the NLP that results from adaptive LGR collocation as shown in Section 3.1. The first and second derivatives with respect to the control are computed using the already computed first and second derivatives required by the NLP solver

$$\frac{\partial \mathcal{H}}{\partial U} = \phi(\mathbf{X}, \boldsymbol{\lambda}, t(\tau, t_0, t_f)), \quad (43)$$

$$\frac{\partial^2 \mathcal{H}}{\partial U^2} = \Phi(\mathbf{X}, \boldsymbol{\lambda}, t(\tau, t_0, t_f)). \quad (44)$$

First, the values of Eq. (44) must be zero. If this condition is satisfied then Eq. (43) is analyzed as follows. A bang-bang interval in the control structure will occur when the switching function ϕ changes sign. The sign of the switching function ϕ is checked in each interval $[d_i, d_{i+1}]$, $i = 1, \dots, n_d$. If the sign in the interval is positive, the control is constrained to its minimum value. If the sign in the interval is negative, the control is constrained to its maximum value. Additional details on these constraints are discussed in Section 5.3.1.

A singular interval in the control structure will occur when the switching function ϕ is zero at every point in the interval $[d_i, d_{i+1}]$. Assessing if the switching function ϕ is zero over the current interval is not a trivial task. Due to the NLP being ill-conditioned when a singular arc is present, the estimated solution over a singular interval will suffer from larger numerical error. The user-defined zero threshold becomes critical in detecting the presence of a singular arc since the switching function will never be exactly zero. In practice, a zero threshold of approximately 10^{-8} has produced accurate results in detecting singular arcs. This threshold is heavily influenced by the coarseness of the initial mesh and the accuracy of the detected discontinuity locations. Once a singular arc has been detected additional constraints in the form of the proximal method are applied as shown in Section 5.3.2. If a scenario occurs where the entire control is singular on $[t_0, t_f]$, then

no discontinuities will be detected. In this situation, the Hamiltonian detection is applied over the entire time domain so that the singular arc can be detected.

5.2 Structure Decomposition

Assuming the structure detection method of Section 5.1 has identified discontinuities and intervals of non-smoothness, the structure decomposition process may be employed. Once acquired, the detected structure of the nonsmooth control is used to introduce the appropriate number of domain interface variables, $t_s^{[d]}$, $s = 1, \dots, S$, $d = [1, \dots, D-1]$, to be solved for on subsequent mesh iterations, where the initial guess for each variable is the estimated discontinuity location that was found using the method in Section 5.1.1. The domain interface variables are included in the NLP by adding them as additional decision variables between the newly created domains, $\mathcal{P}_d = [t_s^{[d-1]}, t_s^{[d]}]$, $d = [1, \dots, D]$. Specifically, the domain interface variables are employed by dividing the time horizon $t \in [t_0, t_f]$ of the original optimal control problem into D domains as described in Section 3.

Next, bounds on the domain interface variables are enforced to prevent the collapse or overlap of domains. Additionally, the bounds provide an additional constraint on the new decision variables. The upper and lower bounds on each domain interface variable are determined by taking the uncertainty bounds found in Section 5.1.1 and transforming them to the time interval $t \in [t_0, t_f]$ using the transformation in Eq. (13). Thus, the bounds $\{d_i^-, d_i^+\}$, $i = 1, \dots, n_d$ are transformed to $\{t_l^{[d]}, t_u^{[d+1]}\}$, $d = [1, \dots, D-1]$.

The nonsmooth optimal control problem has now effectively been partitioned into a multiple domain optimal control problem of the form described in Section 3 where the switch points are represented by the strategically placed domain interface variables $t_s^{[d]}$, $d \in \{1, \dots, D-1\}$. A schematic for the process of decomposing the nonsmooth control structure into a multiple-domain formulation with added variables is shown in Fig. 2. Additionally, the structure of the control has been classified as bang-bang, singular, or smooth. Next, the constraints and refinement strategies required by each type of domain are discussed.

5.3 Domain Constraints and Refinement

Now that structure detection and decomposition has taken place by the methods of Section 5.1 and 5.2, additional constraints are required to properly constrain the multiple-domain optimal control problem. Recall

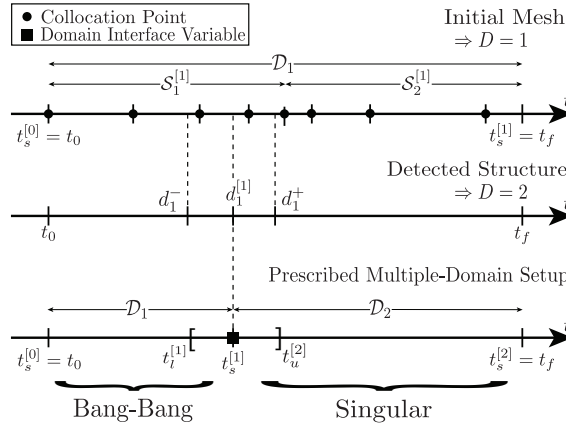


Figure 2: Schematic of process for decomposing the nonsmooth optimal control problem into D domains where the S domain interface variables are included as optimization variables to determine the optimal switch points in the control.

that there are three types of domain classifications: bang-bang, singular, and smooth. Each domain type requires its own set of constraints and refinement methods that are detailed in the following sections.

5.3.1 Bang-Bang Domain Refinement

Suppose the problem has been partitioned into D domains based on the results of structure detection, and it has been determined that \mathcal{B} domains are bang-bang by the method of Section 5.1.2, where $\mathcal{B} < D$. The value of the switching function ϕ in the current domain of interest \mathcal{P}_d is used to determine the value of the control over that domain. Recall, that the switching function assigns the value of the control according to

$$\begin{aligned} u^{[d]}(\tau) &= U_{\min} \quad , \quad \phi^{[d]}(\mathbf{X}, \boldsymbol{\lambda}, t(\tau, t_0, t_f)) > 0, \\ u^{[d]}(\tau) &= U_{\max} \quad , \quad \phi^{[d]}(\mathbf{X}, \boldsymbol{\lambda}, t(\tau, t_0, t_f)) < 0. \end{aligned} \tag{45}$$

The control is then constrained to its corresponding maximum or minimum value in the resulting multiple-domain optimal control problem. The bang-bang control is now appropriately constrained over its domain and the corresponding domain interface variables can be optimized to the optimal switch point locations.

5.3.2 Singular Domain Refinement

The proximal method, see [42], is employed in a singular domain. Assume the problem has been partitioned into D domains based on the results of structure detection, and it has been determined that \mathcal{K} domains are

singular by the method of Section 5.1.2, where $\mathcal{K} < D$ and $\mathcal{K} + \mathcal{B} < D$. Consider one \mathcal{K} domain on the interval $t \in [t_s^{[d-1]}, t_s^{[d]}] = [t_0, t_f]$. The singular domain is transformed into a nonsingular domain through regularization of the singular control. The nonsmooth cost functional is augmented only over the \mathcal{K} -th domain with the penalty term

$$\delta = \frac{\epsilon}{2} \int_{t_0}^{t_f} \left(\frac{u(t) - \alpha_p(t)}{v} \right)^2 dt, \quad (46)$$

that is a function of the singular control and the corresponding approximated control function, $\alpha(t) \in \mathbb{R}$. This augmentation forces the Hamiltonian to become quadratic in the control resulting in a nonsingular well-conditioned NLP. The parameter, ϵ , is a weighting parameter that is a user-defined constant chosen based a parameter study. The parameter, ϵ , cannot be made too large or too small. If the parameter is too small the control will not appear at all in the nonsingular transformation of the problem. If the parameter is too large the added penalty term on the control will over power the cost objective changing the objective function completely. The constant $v \in \mathbb{R}$ is defined as

$$v = \max_{t \in [t_0, t_f]} (|\alpha(t)| + 1), \quad (47)$$

and is a normalization of the penalty term on the interval $[0, 1]$. This normalization is necessary to keep the order of the penalty term consistent with the magnitude of the control. The function $\alpha(t)$ is a piecewise continuous representation of the previous control solution. The continuous representation is achieved by fitting a piecewise cubic polynomial to the previous control solution that satisfies the established properties of a piecewise cubic interpolant stated in [54], thus, guaranteeing a continuous representation of the control. Finally, p represents the current iteration of the proximal method. After the initial solution is obtained, $\alpha(t)$ is initially set to zero for the first iteration ($p = 1$) of the proximal method. On the second iteration $\alpha(t)$ is computed using the previous control solution, $u_{p=1}(t)$.

The augmented multiple-domain optimal control problem to be solved in the proximal method can now be stated. Minimize the cost

$$\mathcal{J} = \mathcal{M}(\mathbf{x}(t_0), t_0, \mathbf{x}(t_f), t_f) + \int_{t_0}^{t_f} [\mathcal{L}(\mathbf{x}(t), u(t), t)] dt + \frac{\epsilon}{2} \int_{t_0}^{t_f} \left(\frac{u(t) - \alpha_p(t)}{v} \right)^2 dt. \quad (48)$$

subject to the dynamics, boundary conditions, and path constraints of Eqs. (2)–(4) and (29). On the next mesh iteration, $M = 2$ and $p = 1$, the augmented version of the newly partitioned optimal control problem resulting from Section 5.2 is solved with $\alpha_p(t) = 0$. Then, on the next iteration $M = 3$ and $p = 2$, the value of

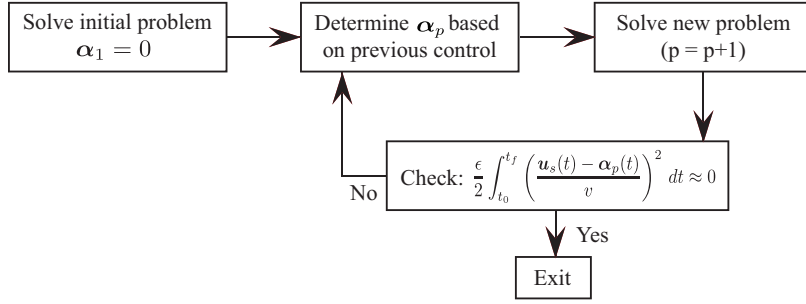


Figure 3: Description of the proximal method during mesh refinement iteration, M .

$\alpha_{p+1}(t)$ is determined based on the previous control solution. After a solution is obtained on each iteration, the penalty term, δ , is checked for convergence. Convergence is achieved when the value of δ is equal to or less than some user defined number, σ . Figure 3 demonstrates how the proximal method is enforced over each mesh refinement iteration in a singular domain.

The objective of the proximal method is to drive the difference between the singular control, $u(t)$, and the approximated control, $\alpha(t)$, in the added penalty term to zero. It has been shown that as $p \rightarrow \infty$ the solution of the augmented problem in Eqs. (48), (2)–(4) and (29) approaches the singular solution of the original optimal control problem [34]. In order to recover the solution to the original optimal control problem, $u^*(t) = \alpha_p(t)$; however, in practice near-zero values are sufficient to achieve an approximate, but nearly optimal solution. If the solution is exact, it would lead to numerical issues in the NLP solver that stem from the original ill-conditioned NLP.

It should be noted that the proximal method described here can be extended to \mathcal{K} domains, but for simplicity the mathematical formulation is presented for one singular domain. Furthermore, the formulation is also presented for a scalar control, but can be extended to multiple control components as later shown in the examples of Section 7.

5.3.3 Smooth Domain Refinement

Suppose one or all domains \mathcal{P}_d are determined to be smooth, meaning the domain is neither bang-bang nor singular. In its current state, the initial mesh has been partitioned into D domains where S domain interface variables have been assigned and corresponding constraints and methods have been applied. Furthermore, the mesh intervals on the initial solution have been remapped to the new domains as well. However, the domains

that are classified as being smooth will contain mesh intervals that may need to be refined. Refinement is applied if the current solution's maximum relative error does not meet the user-defined mesh tolerance. Details on how the mesh error is evaluated can be found in [21].

There are multiple methods existing in the literature to fulfill the role of smooth mesh refinement, but this research refines the mesh on a smooth domain using the method method in [21]. For a more detailed explanation of how smooth mesh refinement works, see [21], as the focus of this research is on structure refinement for nonsmooth optimal control problems.

6 Algorithm

An overview of the proposed algorithm appears below. The mesh refinement iteration is denoted by M and is incremented by one with each loop of the algorithm. The proximal refinement iteration is denoted by p and is incremented by one on each mesh iteration as required by the proximal method. This algorithm terminates when two requirements are met. First, the objective penalty term (46) must be within a user specified tolerance σ from zero, or if Eq. (46) remains identical in value over three consecutive iterations. Second, the mesh error tolerance, e , must be satisfied on each mesh interval or if M reaches a prescribed limit, M_{\max} . The method is executed as follows:

Method for Solving Bang-Bang and Singular Optimal Control Problems

Step 1: Set $M = 0$ and specify initial mesh. All mesh intervals form a single domain.

Step 2: Solve NLP of Section 3 on mesh M .

Step 3: Compute relative error e on current mesh M .

Step 4: If $e_{\max} \leq e$ or $M > M_{\max}$, then quit. Otherwise go to **Step 5**.

Step 5: If $M < 1$ then go to **Step 6**. Otherwise:

(a): If $\delta > \sigma$, then quit.

(b): Set $\alpha_{p+1}(t) = u_p^*(t)$.

(c): Set $\mathbf{x}_{p+1}(t) = \mathbf{x}_p^*(t)$, $u_{p+1}(t) = u_p^*(t)$, and $t_{s_{p+1}}^{[d]} = t_{s_p}^{[d]*}$, $d \in \{1, \dots, D-1\}$, $s \in \{1, \dots, S\}$.

(d): Increment $M \rightarrow M+1$ and return to **Step 2**

Step 6: If $M = 1$, determine the number of switch points, S , using the methods of Section 5.1.

Step 7: If $S = 0$ or $M > 1$, apply smooth mesh refinement and proceed to **Step 9**.

Step 8: If $S > 0$ and $M = 1$, employ the method developed in Section 5 using the following steps:

(a): Classify the intervals as bang-bang or singular using the method of 5.1.2.

(b): Assign S domain interface variables by method of Section 5.2.

(c): Partition time horizon into multiple domains ($D = S+1$) by method of Section 5.2.

(d): Perform domain refinement according to Section 5.2.

(i): Enforce control constraints in each bang-bang domain as in Section 5.3.1.

(ii): Employ proximal method in singular domains according to Section 5.3.2.

(iii): Apply smooth mesh refinement in smooth domains as in Section 5.3.3.

Step 9: Increment $M \rightarrow M+1$ and return to **Step 2**.

7 Numerical Examples

In this section, four nontrivial bang-bang and singular optimal control problems are solved using the method described in Section 5. Each of the four problems demonstrates the methods abilities to solve different types of nonsmooth optimal control problems including a purely bang-bang control, a bang-singular control where the analytic solution exists, a bang-singular-bang control with no analytic solution, and finally a problem with both a finite and infinite-order singular arc as well as bang-bang arcs across multiple control components.

The following conventions are used for all of the examples. The proposed method for solving bang-bang and singular optimal control problems developed in Section 5 is referred to as the BBSOC method. The example problems are also solved using `GPOPS-III` [55] which employs standard LGR collocation and hp -

adaptive smooth mesh refinement [21], and is referred to as *hp*-LGR. Furthermore, the BBSOC method is validated for each example using either the analytic solution, if it exists, or a numerically correct solution obtained using the optimality conditions presented in Section 2. All results are obtained using MATLAB and the nonlinear program developed in Section 3 is solved using IPOPT [2] in full-Newton mode. The NLP solver tolerance is set to 10^{-8} and the mesh refinement tolerance for smooth mesh refinement, see [55], is set to 10^{-8} . All first and second derivatives are supplied to IPOPT using the automatic differentiation software ADiGator [56]. The initial mesh is set to a standard 10×4 mesh meaning the mesh has ten intervals with four collocation points in each interval. Finally, all computations were performed on a 2.9 GHz 6-Core Intel Core i9 MacBook Pro running macOS Big Sur Version 11.1 with 32 GB 2400 MHz DDR4 of RAM, using MATLAB version R2019b (build 9.7.0.1190202) and all computation (CPU) times are in reference to this aforementioned machine.

7.1 Example 1: Robot Arm Problem

Consider the following problem where the goal is to reorient a robotic arm in minimum time [57]:

$$\begin{aligned} & \text{minimize} \quad \mathcal{J} = t_f, \\ & \text{subject to} \quad \left\{ \begin{array}{ll} y_1 = y_2 & , \quad y_1(0) = 9/2 \quad , \quad y_1(t_f) = 9/2, \\ y_2 = u_1/L & , \quad y_2(0) = 0 \quad , \quad y_2(t_f) = 0, \\ y_3 = y_4 & , \quad y_3(0) = 0 \quad , \quad y_3(t_f) = 2\pi/3, \\ y_4 = u_2/I_\theta & , \quad y_4(0) = 0 \quad , \quad y_4(t_f) = 0, \\ y_5 = y_6 & , \quad y_5(0) = \pi/4 \quad , \quad y_5(t_f) = \pi/4, \\ y_6 = u_3/I_\phi & , \quad y_6(0) = 0 \quad , \quad y_6(t_f) = 0, \\ -1 \leq u_i \leq 1, \quad (i = 1, 2, 3) \quad , \end{array} \right. \quad (49) \end{aligned}$$

where t_f is free, $I_\phi = \frac{1}{3}((L - y_1)^3 + y_1^3)$, $I_\theta = I_\phi \sin^2(y_5)$, and $L = 5$. The robot arm problem has a bang-bang structure among its three control components where the bang arcs are defined by five switch points in the control profile.

The control solution obtained when solving this problem using the BBSOC and *hp*-LGR methods are shown in Fig. 4. Observing the controls in Figs. 4a–4c, it is seen that the all five switch points are iden-

Table 1: Comparison of computational results for Example 1.

	$t_s^{[1]}$	$t_s^{[2]}$	$t_s^{[3]}$	$t_s^{[4]}$	$t_s^{[5]}$	$\mathcal{J}^* = t_f$	CPU [s]
BBSOC	2.2852279	2.7960432	4.5704559	6.3448686	6.8556838	9.1409117	2.7984
<i>hp</i> -LGR	2.2498130	2.7950309	4.5182930	6.3306913	6.8203049	9.1409838	3.2461

tified and the controls are constrained to their corresponding boundaries after one iteration of the BBSOC method. In contrast, the *hp*-LGR method does not correctly identify all five discontinuities and as a result obtains incorrect solutions of the controls. The *hp*-LGR method attempts to place more collocation points surrounding the switch points resulting in a higher dimensional problem that still fails to identify the exact locations of the control switches. It can be seen in Table 1 that the BBSOC method produces high-accuracy approximations of the switch points and objective while the *hp*-LGR method fails to achieve the same precision. The computation times for both methods are also compared in Table 1. The BBSOC method converges to the correct solution faster than the *hp*-LGR method. Next, Fig. 4d shows the switching functions that correspond to each of the control components. These switching functions are obtained using the initial control solution and are used to identify the boundary that the control should be constrained to in each domain.

7.2 Example 2: Aly Problem

Consider the following linear-quadratic regulator problem presented in [58]:

$$\begin{aligned}
 & \text{minimize} \quad \mathcal{J} = \frac{1}{2} \int_0^{t_f} (x_1^2(t) + x_2^2(t)) dt, \\
 & \text{subject to} \quad \begin{cases} \dot{x}_1 = x_2 & , \quad x_1(0) = 0 & , \quad x_1(t_f) = \text{Free}, \\ \dot{x}_2 = u & , \quad x_2(0) = 1 & , \quad x_2(t_f) = \text{Free}, \\ -1 \leq u \leq 1 & , \end{cases} \end{aligned} \tag{50}$$

where the final time is fixed, $t_f = 5$. Furthermore, the analytic solution to the Aly problem exists and can be used to assess the accuracy of the BBSOC method. The analytic solution is obtained using the calculus of variations shown in Section 2, and further details can be found in [58]. The singular control is derived as $u_{\text{sing}}^*(t) = x_1(t)$ and the analytic switch point is listed in Table 2.

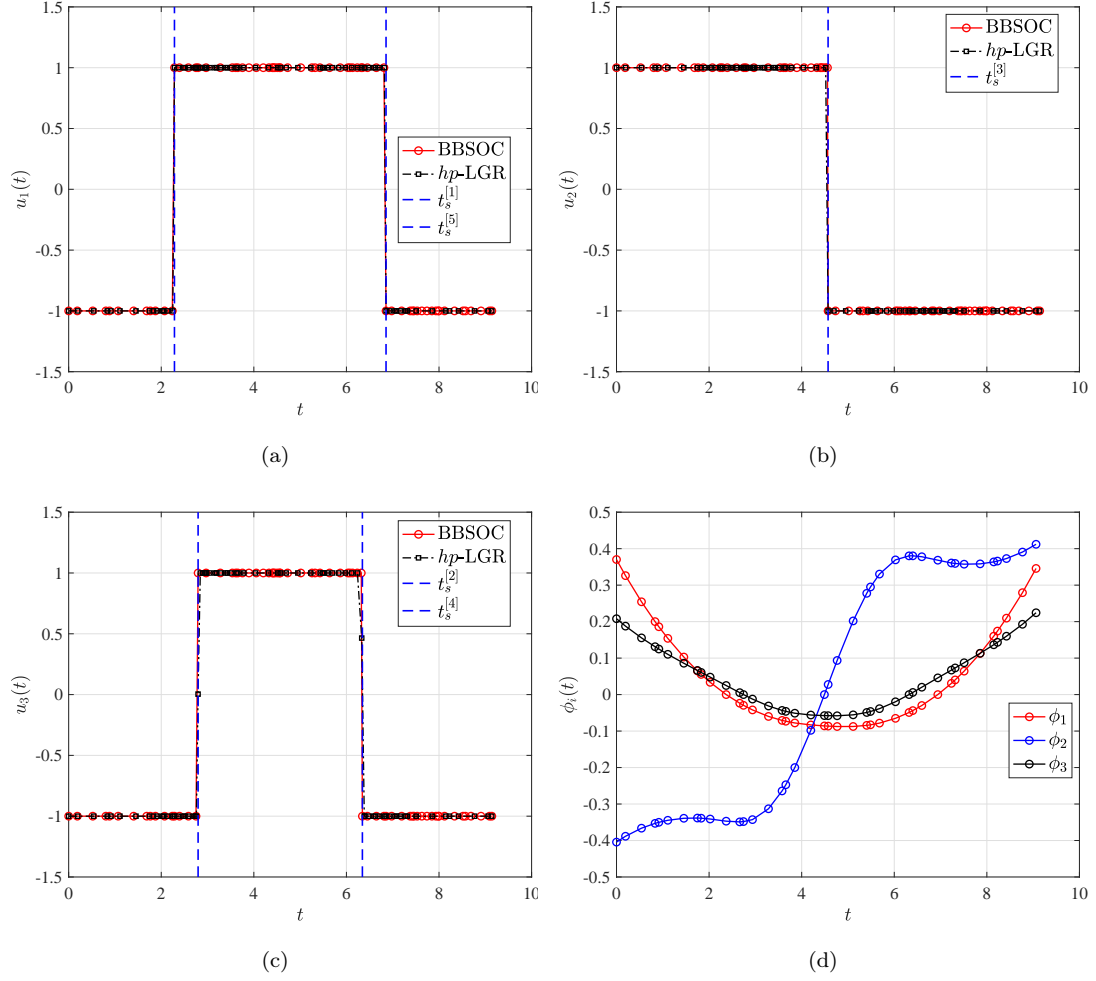


Figure 4: Control component solutions for Example 1 and the corresponding switching functions obtained by the BBSOC method and hp -LGR.

Table 2: Comparison of computational results for Example 2

	$t_s^{[1]}$	\mathcal{J}^*	δ	ϵ	p	CPU [s]
BBSOC	1.41376404	0.37699193	6.31×10^{-14}	10^{-8}	2	4.7541
<i>hp</i> -LGR	1.41194167	0.37699503	—	—	—	2.1251
Analytical	1.41376409	—	—	—	—	—

The control solution obtained when solving this problem using the BBSOC and *hp*-LGR methods are shown in Fig. 5. In Fig. 5a, it is seen that the switch point is identified and the singular control is approximated to a high-accuracy after two iterations of the BBSOC method. In contrast, the *hp*-LGR method obtains a solution that exhibits oscillations at the location of the switch point. These oscillations are caused by the ill-conditioning of the NLP that results from the Hessian matrix not being positive-definite. Figure 5b shows the history of the control obtained on each iteration of the proximal method. These oscillations are inevitably removed by the BBSOC method after two iterations of the proximal method as shown in Fig. 5b.

Next, Table 2 also provides a comparison of the switch point and objective function values obtained using both methods and are also compared to the analytical solution. The value of the analytical switch point is in close agreement with the switch point obtained from the BBSOC method validating the performance of the BBSOC method. The user-defined parameters for the proximal method are also included in Table 2. The computation times for both methods are also compared in Table 2. The BBSOC method takes twice as long as the *hp*-LGR method to converge, but it produces a far more accurate solution. Finally, Fig. 5c shows the switching function that corresponds to the control. This switching function is obtained using the initial control solution and is used to identify the boundary that the control should be constrained to in each domain. The switching function is also provided in Fig. 5c to show when the function switches from positive values to zero, indicating a singular arc is present.

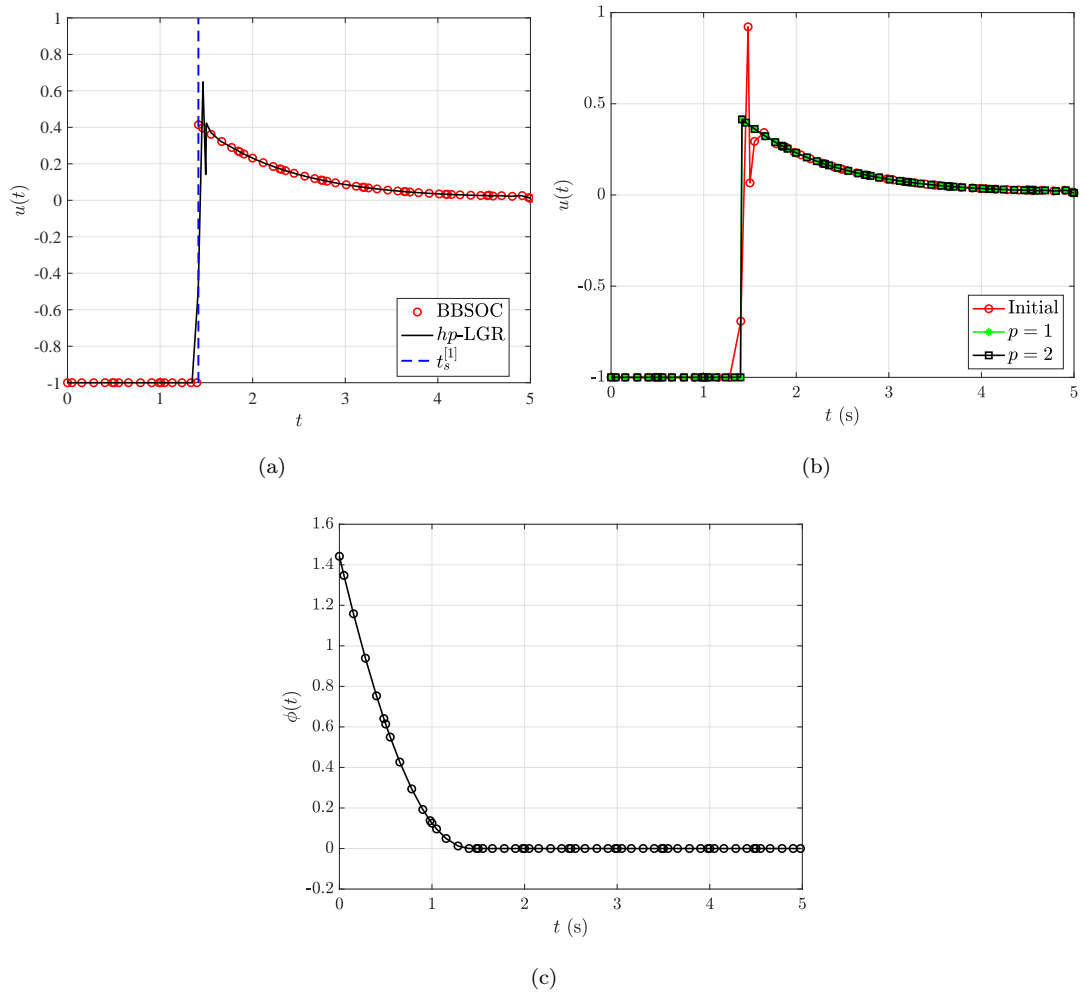


Figure 5: Control solution for Example 2 and the corresponding switching function obtained by the BBSOC method and hp -LGR.

7.3 Example 3: Goddard Rocket Problem

Consider the Goddard rocket problem [45]:

$$\begin{aligned} & \text{minimize} \quad \mathcal{J} = -h(t_f), \\ & \text{subject to} \quad \begin{cases} \dot{h} = v & , \quad h(0) = 0 \quad , \quad h(t_f) = \text{Free}, \\ \dot{v} = \frac{T-D}{m} - g & , \quad v(0) = 0 \quad , \quad v(t_f) = \text{Free}, \\ \dot{m} = -\frac{T}{c} & , \quad m(0) = 3 \quad , \quad m(t_f) = 1, \\ 0 \leq T \leq T_{\max} & , \end{cases} \end{aligned} \quad (51)$$

where h is the altitude, v is the velocity, m is the mass, T is the thrust (i.e. control), $D = D_0 v^2 \exp(-h/H)$, and the final time is free. Further details on the model and the parameters can be found in Ref. [45]. Furthermore, it is known that the singular control law can be obtained by taking time derivatives of the optimality condition, \mathcal{H}_u , until the control explicitly appears. The following singular arc law is derived

$$T_{\text{sing}} = D + mg + \left[\frac{c^2(1 + \frac{v}{c})}{Hg} - 1 - \frac{2c}{v} \right] \left[\frac{mg}{1 + \frac{4c}{v} + \frac{2c^2}{v^2}} \right]. \quad (52)$$

Given that the singular control can be found analytically, it should be possible to obtain the numerically exact solution to this example using a three-phase optimal control problem with the singular control enforced as a path constraint in the second phase. This numerically exact solution, referred to as the *baseline* solution, is shown in Fig. 6 and obtained using `GPOPS-III` [55].

The problem in Eq. (51) is solved using the BBSOC and *hp*-LGR methods. Both of these solutions are compared in Fig. 6a and parameters related to the proximal method are provided in Table 3. Figure 6a demonstrates that the proximal method has converged to the correct singular control while also correctly identifying the switch times in the control. In contrast, the *hp*-LGR method obtains a solution that exhibits oscillations at the switch points defining the singular arc. These oscillations are also seen in the initial iterations of the proximal method, but are removed by the fifth iteration as seen in Fig. 6b.

Next, Table 3 compares the solution obtained using the BBSOC method, the *hp*-LGR method, and the baseline solution. These results further validate the BBSOC methods ability to identify the optimal switch points, final time, and obtain a high-accuracy approximation of the singular control. The BBSOC results are also in close agreement with the baseline solution. In contrast, the *hp*-LGR results are not in agreement with the baseline solution. The computation times for all three methods are also compared in Table 3. The

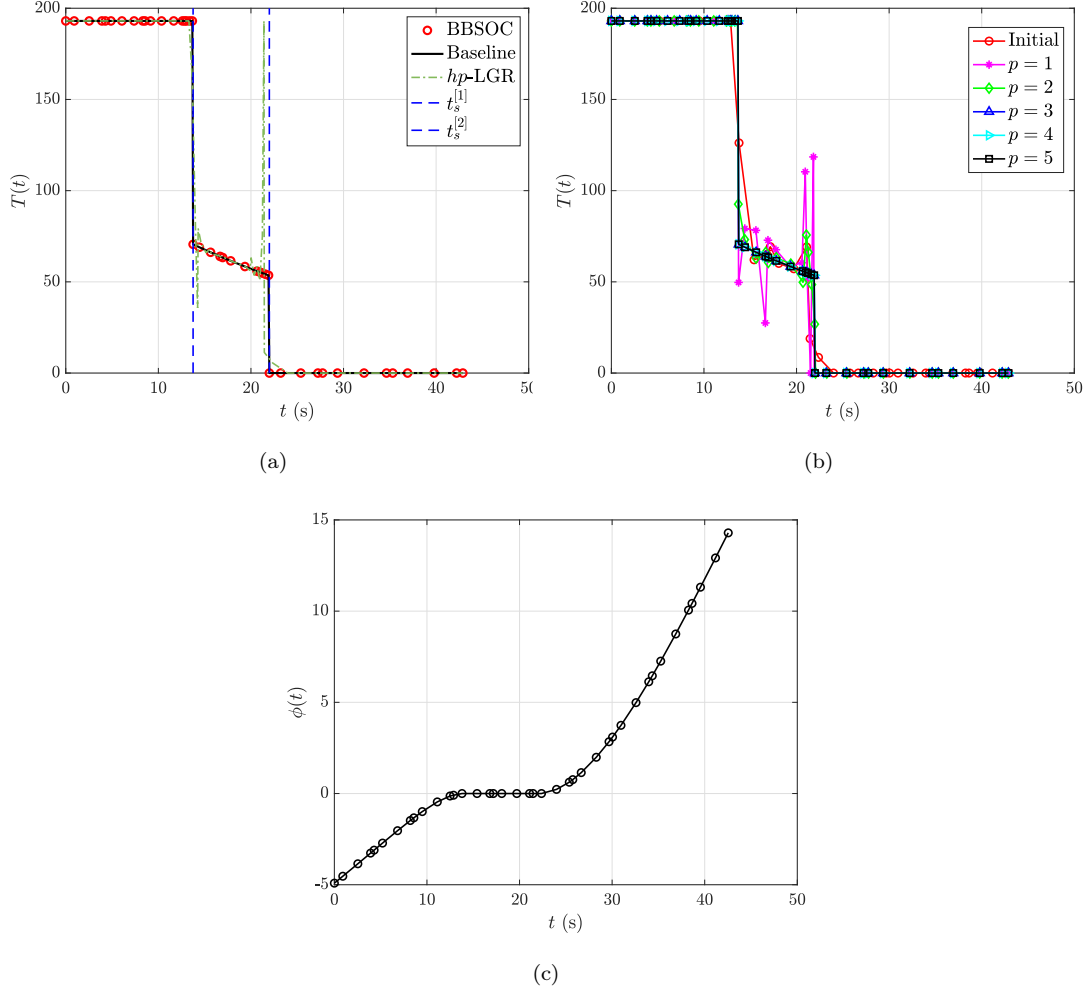


Figure 6: Control solution for Example 3 and the corresponding switching function obtained by the BBSOC method, hp -LGR, and $\mathbb{GPOPS} - \text{III}$.

BBSOC method takes twice as long as the hp -LGR method to converge, but it produces a far more accurate solution. Although the BBSOC method also takes twice as long as the baseline solution to converge, the BBSOC method achieved the same accuracy without any a priori knowledge of the singular problem. Finally, Fig. 6c shows the switching function that corresponds to the control. This switching function is obtained using the initial control solution and is used to identify the boundary that the control should be constrained to in each domain. The switching function is also provided in Fig. 6c to show when the function switches from positive values to zero, indicating a singular arc is present.

Table 3: Comparison of computational results for Example 3.

	$t_s^{[1]}$	$t_s^{[2]}$	t_f	$\mathcal{J}^* = -h(t_f)$	δ	ϵ	p	CPU [s]
BBSOC	13.751085	21.987784	42.887912	18550.87189	7.86×10^{-8}	10^{-6}	4	4.7364
<i>hp</i> -LGR	13.541287	22.213037	42.887750	18550.87039	—	—	—	2.2387
Baseline	13.751270	21.987363	42.887912	18550.87186	—	—	—	2.5686

7.4 Example 4: Minimum Time Reorientation of a Spacecraft

Consider the following optimal control problem where the objective is to reorient a spacecraft from an initial altitude, with some angular velocity, to a final altitude with a specified angular velocity in minimum time [59]:

$$\begin{aligned}
 & \text{minimize} \quad \mathcal{J} = t_f, \\
 & \text{subject to} \quad \left\{ \begin{array}{l} \dot{\omega}_1 = a\omega_{30}\omega_2 + u_1, \quad \omega_1(0) = \omega_{1_0}, \quad \omega_1(t_f) = \omega_{1_f}, \\ \dot{\omega}_2 = -a\omega_{30}\omega_1 + u_2, \quad \omega_2(0) = \omega_{2_0}, \quad \omega_2(t_f) = \omega_{2_f}, \\ \dot{x}_1 = \omega_{30}x_2 + \omega_2x_1x_2 + \frac{\omega_1}{2}(1 + x_1^2 - x_2^2), \quad x_1(0) = x_{1_0}, \quad x_1(t_f) = x_{1_f}, \\ \dot{x}_2 = \omega_{30}x_1 + \omega_1x_1x_2 + \frac{\omega_2}{2}(1 + x_2^2 - x_1^2), \quad x_2(0) = x_{2_0}, \quad x_2(t_f) = x_{2_f}, \\ |u_i| \leq u_{i,\max}, \quad i = 1, 2 \end{array} \right., \end{aligned} \tag{53}$$

where $\omega_i(t)$ is the angular velocity, $x_i(t)$ is the position of the spacecraft, ω_{30} is the initial condition for $\omega_3(t)$ which remains constant, and $u_{i,\max} = 1$. For the purposes of showing off the capabilities of the method, two special scenarios of the aforementioned spacecraft reorientation problem will be shown. These two scenarios include the case of a nonspinning axisymmetric rigid body and the case of an inertially symmetric rigid body. Full details of the singular arc analysis can be found in [59], but for the purpose of this work the first scenario results in a second-order singular arc and the second scenario results in an infinite-order singular arc.

7.4.1 Nonspinning Axisymmetric Body ($\omega_{30} = 0$)

For this scenario, a second-order singular arc occurs for the boundary conditions $(\omega_{1_0}, \omega_{2_0}, x_{1_0}, x_{2_0}) = (-0.45, -1.1, 0.1, -0.1)$ and $(\omega_{1_f}, \omega_{2_f}, x_{1_0}, x_{2_0}) = (0, 0, 0, 0)$. The parameters are $a = 0.5$ and $\omega_{30} = 0$.

Table 4: Comparison of computational results for Example 4-1.

	$t_s^{[1]}$	$t_s^{[2]}$	$t_s^{[3]}$	$t_s^{[4]}$	$t_s^{[5]}$	$\mathcal{J}^* = t_f$	δ	ϵ	p	CPU [s]
BBSOC	0.6498	1.2898	1.8188	1.9084	1.9919	2.8839	1.24×10^{-10}	10^{-3}	2	3.3739
<i>hp</i> -LGR	0.6498	1.2897	1.8184	1.9226	1.9922	2.8839	—	—	—	5.1750
Shen [59]	0.6489	1.2925	1.8073	1.9040	2.0000	2.8800	—	—	—	—

The first control has a *bang-singular* structure and the second control is *bang-bang*. The physical representation of this scenario is to reorient the body until the symmetry axis is aligned with the inertial axis, representing the body in a rest situation.

The control solutions obtained when solving the problem using the BBSOC and *hp*-LGR methods are shown in Fig. 7 and they are validated using the results of Shen et. al. [59]. From [59], it is known that $u_{1,\text{sing}}^*(t) = 0$. In fig. 7a and 7b, the singular control is approximated to a high-accuracy and the five switch points are identified using the BBSOC method. In contrast, the *hp*-LGR method obtains a control solution that exhibits oscillatory behavior due to the ill-conditioning of the NLP. Figure 7e plots each control solution at every iteration of the proximal method to show how the BBSOC method efficiently eliminates the oscillations in the initial control solution.

Next, Table 4 provides the switch point locations and final time obtained by each of the three methods along with the parameters required for the proximal method. While the switch points obtained by each method seem to be in excellent agreement, the actual control profiles obtained are not as explained previously. Finally, Figs. 7c and 7d show the switching functions that correspond to each of the control components. This switching functions are obtained using the initial control solution and are used to identify the boundary that the control should be constrained to in each domain. The switching functions also indicate the presence of a bang-bang arc and singular arc in the control. The computation times for both methods are also compared in Table 4. The BBSOC converges to a higher accuracy solution faster than the *hp*-LGR method.

7.4.2 Inertially Symmetric Body ($a = 0$)

For this scenario, an infinite-order singular arc is observed for the following boundary conditions $(\omega_{1_0}, \omega_{2_0}, w_{1_0}, w_{2_0}) = (0, 0, 0, 0)$ and $(\omega_{1_f}, \omega_{2_f}, w_{1_0}, w_{2_0}) = (1, 2, \text{Free}, \text{Free})$. The parameters are $a = 0$ and $\omega_{30} = -0.3$.

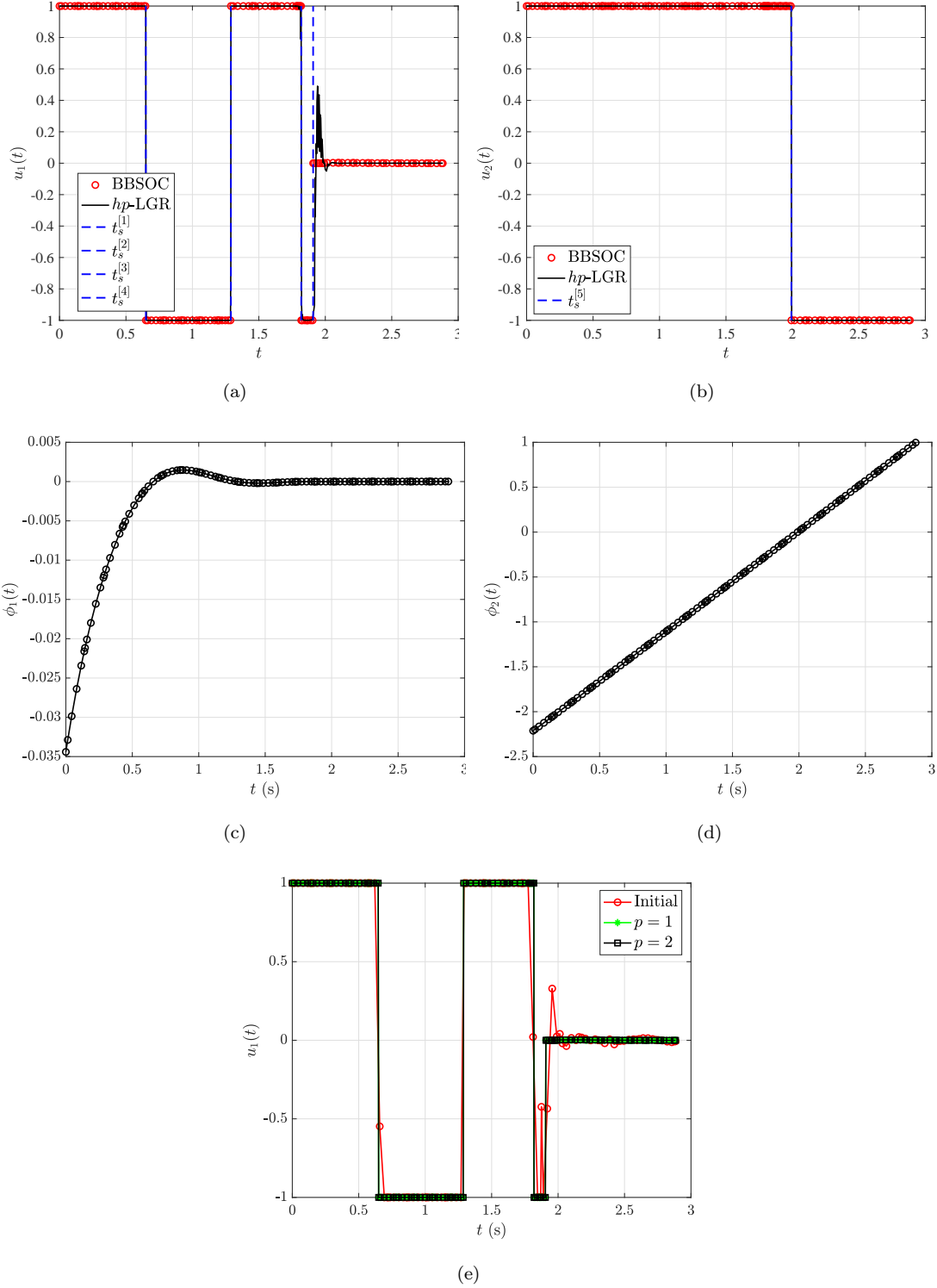


Figure 7: Control component solutions for Example 4-1 and the corresponding switching function obtained by the BBSOC method and hp -LGR.

Table 5: Comparison of computational results for Example 4–2.

	$\mathcal{J}^* = t_f$	δ	ϵ	p	CPU [s]
BBSOC	2.00	1.11×10^{-19}	10^{-1}	2	5.1758
<i>hp</i> -LGR	2.00	—	—	—	1.6347
Shen [59]	2.00	—	—	—	—

The physical meaning of this scenario is to accelerate the angular velocities from zero to their final specified values, respectively, where the final position is not of importance.

For this case, the entire time domain is singular and the problem does not need to be split into domains. As a result the BBSOC method does not assign any domain interface variables and instead the proximal method is applied over the entire, single time domain. From [59], it is known that a solution to the singular control is $u_{1,\text{sing}}^*(t) = 0.5$. Table 5 provides the results obtained using the proximal method, *hp*-LGR and Ref. [59]. It seems that all three solutions are in agreement; however, Fig. 8a shows that the control obtained using *hp*-LGR is actually incorrect. In Fig. 8c, the proximal method converges to the optimal singular control whereas the *hp*-LGR solution exhibits highly oscillatory behavior due to the ill-conditioning of the NLP. The same observations are also made for the second bang-bang control component in Fig. 8b. The control history over each proximal iteration is provided in Fig. 8c. The computation times for both methods are also compared in Table 5. The BBSOC converges to a higher accuracy solution than the *hp*-LGR method, but takes about five times as long. The switching functions are also provided in Fig. 8d to show that the function remains constant at either zero or a negative value, indicating the presence of singular arcs and bang-bang arcs. This case illustrates the BBSOC methods ability to detect and approximate infinite-order singular controls to a high accuracy.

8 Conclusions

A method has been described for solving bang-bang and singular optimal control problems using an adaptive Radau collocation method and regularization of the singular control. First, the solution is approximated on a coarse mesh. Next, structure detection is performed via discontinuity detection and Hamiltonian

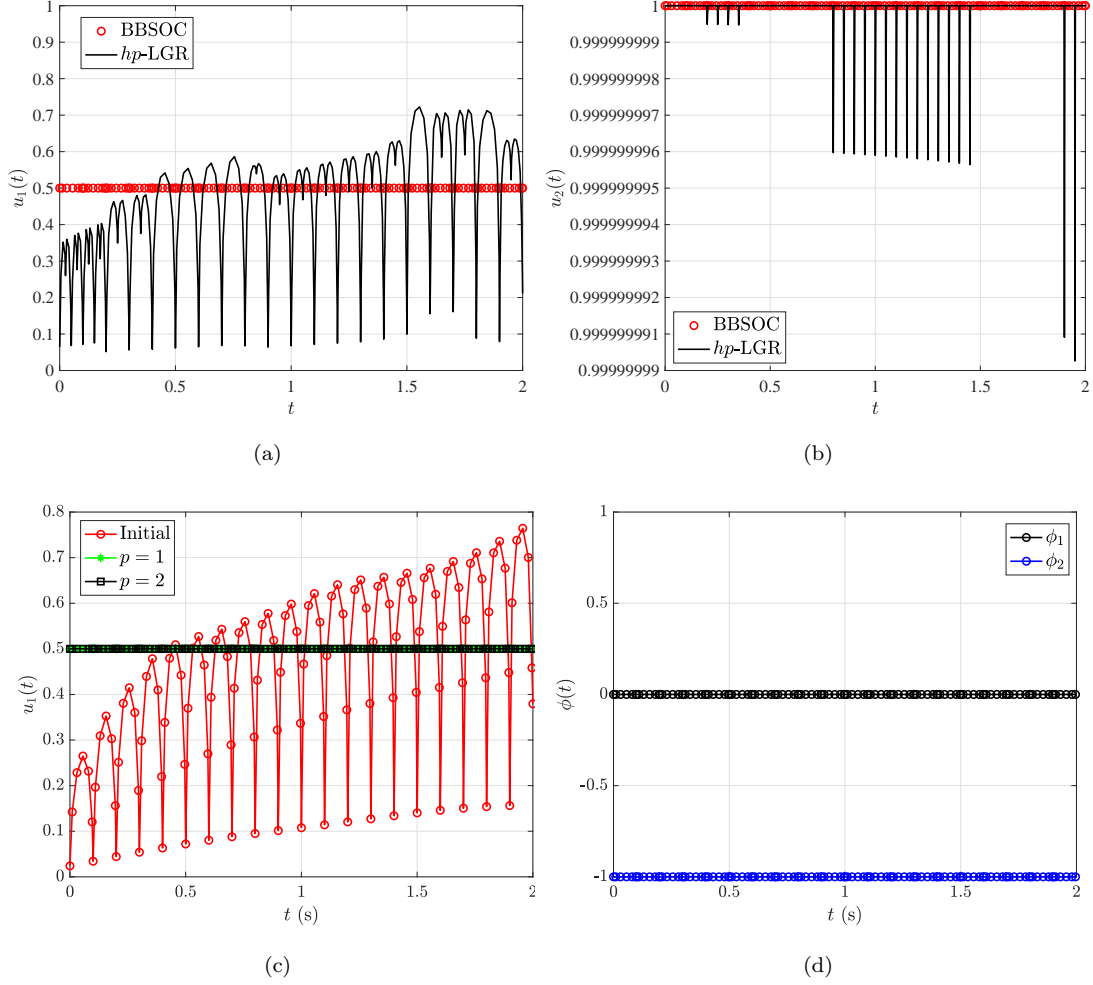


Figure 8: Control component solutions for Example 4-2 and the corresponding switching function obtained by the BBSOC method and hp -LGR.

detection. If the structure detected contains discontinuities and bang-bang and/or singular arcs, the structure is partitioned into a multiple-domain formulation with added decision variables to represent the switch points. Then, corresponding constraints and methodologies are assigned in each domain type. In bang-bang domains the control is fixed at either its upper or lower limit and in a singular domain the proximal method is employed to regularize the singular control. Finally, smooth mesh refinement is performed if necessary. The strategy of this method allows for highly accurate approximations of the switch times and nonsmooth control. The method has been demonstrated on four nontrivial examples where it has been shown to obtain highly accurate approximations to solutions of bang-bang and singular optimal control problems.

9 Acknowledgments

The authors gratefully acknowledge support for this research from Lockheed-Martin Corporation under contract 4104177872 and from the U.S. National Science Foundation under grants DMS-1522629, DMS-1924762, and CMMI-1563225.

References

- [1] Betts, J. T., *Practical methods for optimal control and estimation using nonlinear programming*, SIAM, 2010.
- [2] Biegler, L. T. and Zavala, V. M., “Large-Scale Nonlinear Programming Using IPOPT: An Integrating Framework for Enterprise-Wide Optimization,” *Computers and Chemical Engineering*, Vol. 33, No. 3, March 2008, pp. 575–582.
- [3] Gill, P. E., Murray, W., and Saunders, M. A., “SNOPT: An SQP Algorithm for Large-Scale Constrained Optimization,” *SIAM Review*, Vol. 47, No. 1, January 2002, pp. 99–131.
- [4] Benson, D. A., Huntington, G. T., Thorvaldsen, T. P., and Rao, A. V., “Direct Trajectory Optimization and Costate Estimation via an Orthogonal Collocation Method,” *Journal of Guidance, Control, and Dynamics*, Vol. 29, No. 6, November-December 2006, pp. 1435–1440.
- [5] Garg, D., Patterson, M. A., Hager, W. W., Rao, A. V., Benson, D. A., and Huntington, G. T., “A Unified Framework for the Numerical Solution of Optimal Control Problems Using Pseudospectral Methods,” *Automatica*, Vol. 46, No. 11, November 2010, pp. 1843–1851. DOI: 10.1016/j.automatica.2010.06.048.
- [6] Garg, D., Hager, W. W., and Rao, A. V., “Pseudospectral Methods for Solving Infinite-Horizon Optimal Control Problems,” *Automatica*, Vol. 47, No. 4, April 2011, pp. 829–837. DOI: 10.1016/j.automatica.2011.01.085.
- [7] Garg, D., Patterson, M. A., Darby, C. L., Francolin, C., Huntington, G. T., Hager, W. W., and Rao, A. V., “Direct Trajectory Optimization and Costate Estimation of Finite-Horizon and Infinite-Horizon Optimal Control Problems via a Radau Pseudospectral Method,” *Computational Optimization and Applications*, Vol. 49, No. 2, June 2011, pp. 335–358. DOI: 10.1007/s10589-00-09291-0.

- [8] Rao, A. V., Benson, D. A., Darby, C. L., Francolin, C., Patterson, M. A., Sanders, I., and Huntington, G. T., "Algorithm 902: GPOPS, A MATLAB Software for Solving Multiple-Phase Optimal Control Problems Using the Gauss Pseudospectral Method," *ACM Transactions on Mathematical Software*, Vol. 37, No. 2, April–June 2010, Article 22, 39 pages.
- [9] Kameswaran, S. and Biegler, L. T., "Convergence Rates for Direct Transcription of Optimal Control Problems Using Collocation at Radau Points," *Computational Optimization and Applications*, Vol. 41, No. 1, 2008, pp. 81–126.
- [10] Elnagar, G., Kazemi, M. A., and Razzaghi, M., "The Pseudospectral Legendre Method for Discretizing Optimal Control Problems," *IEEE transactions on Automatic Control*, Vol. 40, No. 10, 1995, pp. 1793–1796.
- [11] Hager, W. W., Hou, H., and Rao, A. V., "Convergence Rate for a Radau Collocation Method Applied to Unconstrained Optimal Control," 2015, [arXiv.org/abs/1508.03783](https://arxiv.org/abs/1508.03783).
- [12] W. W. Hager and H. Hou and A. V. Rao, "Convergence Rate for a Gauss Collocation Method Applied to Unconstrained Optimal Control," *Journal of Optimization Theory and Applications*, Vol. 169, No. 3, June 2016, pp. 801 – 824.
- [13] Hager, W. W., Hou, H., and Rao, A. V., "Lebesgue Constants Arising in a Class of Collocation Methods," *IMA Journal of Numerical Analysis*, Vol. 37, No. 4, October 2017, pp. 1884–1901.
- [14] Hager, W. W., Hou, H., Mohapatra, S., and Rao, A. V., "Convergence Rate for an *hp*-Collocation Method Applied to Unconstrained Optimal Control," "2016, [arXiv.org/abs/1605.02121](https://arxiv.org/abs/1605.02121)".
- [15] Hager, W. W., Mohapatra, S., and Rao, A. V., "Convergence Rate for a Gauss Collocation Method applied to Constrained Optimal Control," "2016, [arXiv.org/abs/1607.02798](https://arxiv.org/abs/1607.02798)".
- [16] Liu, F., Hager, W. W., and Rao, A. V., "Adaptive mesh refinement method for optimal control using nonsmoothness detection and mesh size reduction," *Journal of the Franklin Institute*, Vol. 352, No. 10, oct 2015, pp. 4081–4106.
- [17] Gong, Q., Fahroo, F., and Ross, I. M., "Spectral Algorithm for Pseudospectral Methods in Optimal Control," *Journal of Guidance, Control, and Dynamics*, Vol. 31, No. 3, may 2008, pp. 460–471.
- [18] Miller, A. T., Hager, W. W., and Rao, A. V., "Mesh refinement method for solving optimal control problems with nonsmooth solutions using jump function approximations," *Optimal Control Applications and Methods*, 2021.
- [19] Liu, F., Hager, W. W., and Rao, A. V., "Adaptive Mesh Refinement Method for Optimal Control Using Decay Rates of Legendre Polynomial Coefficients," *IEEE Transactions on Control Systems Technology*, Vol. 26, No. 4, July 2018, pp. 1475–1483.
- [20] Darby, C. L., Hager, W. W., and Rao, A. V., "An *hp*-adaptive pseudospectral method for solving optimal control problems," *Optimal Control Applications and Methods*, Vol. 32, No. 4, Aug. 2010, pp. 476–502.
- [21] Patterson, M. A., Hager, W. W., and Rao, A. V., "A *ph* mesh refinement method for optimal control," *Optimal Control Applications and Methods*, Vol. 36, No. 4, Feb. 2014, pp. 398–421.
- [22] Schlegel, M. and Marquardt, W., "Direct Sequential Dynamic Optimization with Automatic Switching Structure Detection," *IFAC Proceedings Volumes*, Vol. 37, No. 9, July 2004, pp. 419–424.
- [23] Schlegel, M. and Marquardt, W., "Detection and exploitation of the control switching structure in the solution of dynamic optimization problems," *Journal of Process Control*, Vol. 16, No. 3, March 2006, pp. 275–290.
- [24] Wang, P., Yang, C., and Yuan, Z., "The Combination of Adaptive Pseudospectral Method and Structure Detection Procedure for Solving Dynamic Optimization Problems with Discontinuous Control Profiles," *Industrial & Engineering Chemistry Research*, Vol. 53, No. 17, April 2014, pp. 7066–7078.

- [25] Chen, W. and Biegler, L. T., “Nested direct transcription optimization for singular optimal control problems,” *AIChE Journal*, Vol. 62, No. 10, May 2016, pp. 3611–3627.
- [26] Chen, W., Ren, Y., Zhang, G., and Biegler, L. T., “A simultaneous approach for singular optimal control based on partial moving grid,” *AIChE Journal*, Vol. 65, No. 6, March 2019, pp. e16584.
- [27] Agamawi, Y. M., Hager, W. W., and Rao, A. V., “Mesh refinement method for solving bang-bang optimal control problems using direct collocation,” *AIAA Scitech 2020 Forum*, 2020, p. 0378.
- [28] Aghaee, M. and Hager, W. W., “The Switch Point Algorithm,” 2021.
- [29] Kaya, C. and Noakes, J., “Computational Method for Time-Optimal Switching Control,” *Journal of Optimization Theory and Applications*, Vol. 117, No. 1, April 2003, pp. 69–92.
- [30] Mehrpouya, M. A., Oshagh, K.-e., et al., “An efficient numerical solution for time switching optimal control problems,” *Computational Methods for Differential Equations*, 2020.
- [31] Maurer, H., “Numerical solution of singular control problems using multiple shooting techniques,” *Journal of Optimization Theory and Applications*, Vol. 18, No. 2, feb 1976, pp. 235–257.
- [32] Aronna, M. S., Bonnans, J. F., and Martinon, P., “A Shooting Algorithm for Optimal Control Problems with Singular Arcs,” *Journal of Optimization Theory and Applications*, Vol. 158, No. 2, Jan. 2013, pp. 419–459.
- [33] Mehra, R. and Davis, R., “A generalized gradient method for optimal control problems with inequality constraints and singular arcs,” *IEEE Transactions on Automatic Control*, Vol. 17, No. 1, Feb. 1972, pp. 69–79.
- [34] Jacobson, D., Gershwin, S., and Lele, M., “Computation of optimal singular controls,” *IEEE Transactions on Automatic Control*, Vol. 15, No. 1, feb 1970, pp. 67–73.
- [35] Andrés-Martínez, O., Flores-Tlacuahuac, A., Kameswaran, S., and Biegler, L. T., “An efficient direct/indirect transcription approach for singular optimal control,” *AIChE Journal*, Vol. 65, No. 3, Dec. 2018, pp. 937–946.
- [36] Caponigro, M., Ghezzi, R., Piccoli, B., and Trélat, E., “Regularization of chattering phenomena via bounded variation controls,” *IEEE Transactions on Automatic Control*, Vol. 63, No. 7, 2018, pp. 2046–2060.
- [37] Mall, K., Grant, M. J., and Taheri, E., “Uniform Trigonometrization Method for Optimal Control Problems with Control and State Constraints,” *Journal of Spacecraft and Rockets*, Vol. 57, No. 5, Sept. 2020, pp. 995–1007.
- [38] Fabien, B. C., “Indirect Solution of Inequality Constrained and Singular Optimal Control Problems Via a Simple Continuation Method,” *Journal of Dynamic Systems, Measurement, and Control*, Vol. 136, No. 2, nov 2013, pp. 021003.
- [39] Andrés-Martínez, O., Biegler, L. T., and Flores-Tlacuahuac, A., “An indirect approach for singular optimal control problems,” *Computers & Chemical Engineering*, Vol. 139, Aug. 2020, pp. 106923.
- [40] Maga, L., Reverberi, A., et al., “A pattern recognition approach to the solution of optimal singular control problems,” *Chemical Engineering Journal*, Vol. 68, No. 1, 1997, pp. 35–40.
- [41] Pager, E. R. and Rao, A. V., “A Proximal Method for the Numerical Solution of Singular Optimal Control Problems Using a Modified Radau Collocation Method,” *AIAA Scitech 2020 Forum*, American Institute of Aeronautics and Astronautics, Jan. 2020.
- [42] Pager, E. R. and Rao, A. V., “A Method for the Numerical Solution of Singular Optimal Control Problems Using an Adaptive Radau Collocation Method,” *AIAA Scitech 2021 Forum*, American Institute of Aeronautics and Astronautics, Jan. 2021.

- [43] Athans, M. and Falb, P. L., *Optimal control: an introduction to the theory and its applications*, Courier Corporation, 2013.
- [44] Kirk, D. E., *Optimal control theory: an introduction*, Courier Corporation, 2004.
- [45] Bryson, A. E. and Ho, Y., *Applied Optimal Control: Optimization, Estimation, and Control*, Hemisphere Publishing Corporation, 1975.
- [46] Pontryagin, L. S., *Mathematical theory of optimal processes*, Routledge, 2018.
- [47] Bazaraa, M. S., Sherali, H. D., and Shetty, C. M., *Nonlinear programming: theory and algorithms*, John Wiley & Sons, 2013.
- [48] Bertsekas, D. P., Bertsekas, D. P., Bertsekas, D. P., and Bertsekas, D. P., *Dynamic programming and optimal control*, Vol. 1, Athena scientific Belmont, MA, 1995.
- [49] Darby, C. L., Garg, D., and Rao, A. V., “Costate Estimation using Multiple-Interval Pseudospectral Methods,” *Journal of Spacecraft and Rockets*, Vol. 48, No. 5, Sept. 2011, pp. 856–866.
- [50] Tait, K. S., Ph.D. thesis, 1965.
- [51] Kelley, H., Kopp, R. E., and Moyer, H. G., “Topics in Optimization, edited by Leitman,” 1967.
- [52] Kopp, R. E. and Moyer, H. G., “Necessary conditions for singular extremals,” *AIAA Journal*, Vol. 3, No. 8, Aug. 1965, pp. 1439–1444.
- [53] Archibald, R., Gelb, A., and Yoon, J., “Polynomial Fitting for Edge Detection in Irregularly Sampled Signals and Images,” *SIAM Journal on Numerical Analysis*, Vol. 43, No. 1, Jan. 2005, pp. 259–279.
- [54] Fritsch, F. N. and Carlson, R. E., “Monotone Piecewise Cubic Interpolation,” *SIAM Journal on Numerical Analysis*, Vol. 17, No. 2, April 1980, pp. 238–246.
- [55] Patterson, M. A. and Rao, A. V., “GPOPS-II,” *ACM Transactions on Mathematical Software*, Vol. 41, No. 1, oct 2014, pp. 1–37.
- [56] Weinstein, M. J. and Rao, A. V., “Algorithm 984: ADiGator, a Toolbox for the Algorithmic Differentiation of Mathematical Functions in MATLAB Using Source Transformation via Operator Overloading,” *ACM Transactions on Mathematical Software*, Vol. 44, No. 2, Aug. 2017, pp. 1–25.
- [57] Dolan, E. D., More, J. J., and Munson, T. S., “Benchmarking optimization software with COPS 3.0.” Tech. rep., May 2004.
- [58] Aly, G., “The computation of optimal singular control,” *International Journal of Control*, Vol. 28, No. 5, 1978, pp. 681–688.
- [59] Shen, H. and Tsiotras, P., “Time-Optimal Control of Axisymmetric Rigid Spacecraft Using Two Controls,” *Journal of Guidance, Control, and Dynamics*, Vol. 22, No. 5, Sept. 1999, pp. 682–694.